

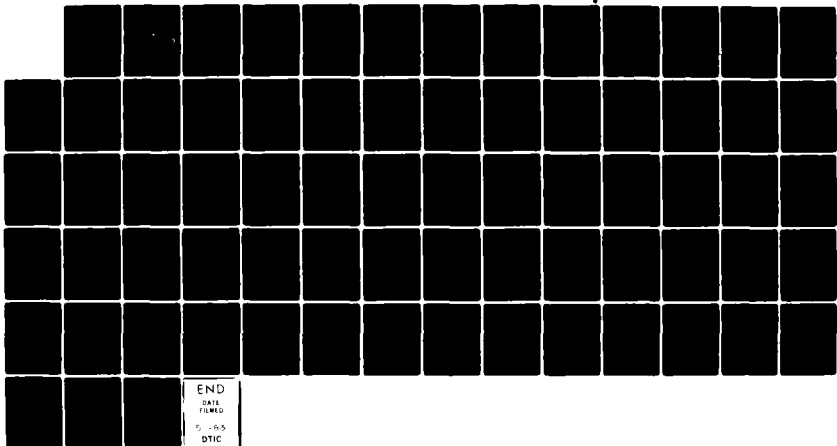
AD-A126 753 CERENKOV RADIATION(U) NAVAL POSTGRADUATE SCHOOL  
MONTEREY CA A SAGLAM DEC 82

1/1

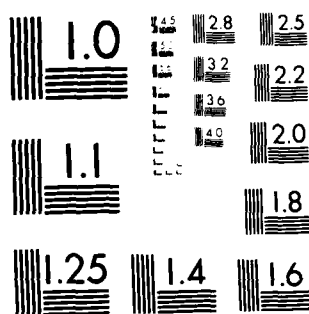
UNCLASSIFIED

F/G 20/8

NL



END  
DATE  
FILED  
FEB - 6 - 83  
DTIC



MICROCOPY RESOLUTION TEST CHART  
NATIONAL BUREAU OF STANDARDS 1967 A

(2)

ADA126759

# NAVAL POSTGRADUATE SCHOOL

## Monterey, California



# THESIS

DTIC  
SELECTED  
APR 11 1983  
H

CERENKOV RADIATION

by

Ahmet Saglam

December 1982

Thesis Advisor:

F. R. Buskirk

Approved for public release; distribution unlimited.

DTIC FILE COPY

UNCLASSIFIED

SECURITY CLASSIFICATION OF THIS PAGE (When Data Entered)

REPORT DOCUMENTATION PAGE		READ INSTRUCTIONS BEFORE COMPLETING FORM
1. REPORT NUMBER	2. GOVT ACCESSION NO.	3. RECIPIENT'S CATALOG NUMBER
		DC AR36 22
4. TITLE (and Subtitle)	5. TYPE OF REPORT & PERIOD COVERED	
Cerenkov Radiation	Master's Thesis; December 1982	
7. AUTHOR(S)	6. PERFORMING ORG. REPORT NUMBER	
Ahmet Saglam		
9. PERFORMING ORGANIZATION NAME AND ADDRESS	10. PROGRAM ELEMENT PROJECT, TASK AREA & WORK UNIT NUMBERS	
Naval Postgraduate School Monterey, California 93940		
11. CONTROLLING OFFICE NAME AND ADDRESS	12. REPORT DATE	
Naval Postgraduate School Monterey, California 93940	December 1982	
14. MONITORING AGENCY NAME & ADDRESS (if different from Controlling Office)	13. NUMBER OF PAGES	
	70	
	15. SECURITY CLASS. (of this report)	
	Unclassified	
	15a. DECLASSIFICATION/DOWNGRADING SCHEDULE	
16. DISTRIBUTION STATEMENT (of info Report)		
Approved for public release; distribution unlimited.		
17. DISTRIBUTION STATEMENT (of the abstract entered in Block 20, if different from Report)		
18. SUPPLEMENTARY NOTES		
19. KEY WORDS (Continue on reverse side if necessary and identify by block number)		
Cerenkov Radiation in air		
20. ABSTRACT (Continue on reverse side if necessary and identify by block number)		
Cerenkov radiation is calculated for electron beams which exceed the velocity of radiation in a nondispersive dielectric medium. The electron beam is assumed to be bunched as emitted from a travelling wave accelerator, and the emission region is assumed to be finite. Predictions include (a) emission at harmonics of the bunch rate, (b) cone angle of radiation at w frequencies, (c) smearing of the emission angle for finite		

**UNCLASSIFIED**

SECURITY CLASSIFICATION OF THIS PAGE/When Data Entered

**#20 - ABSTRACT - (CONTINUED)**

emission regions, (d) explicit evaluation of power spectrum in terms of bunch dimensions. The results of theory are applied to microwave emission from fast electrons in air for different lengths of the air path. Problems encountered during the experiment are discussed and suggestions for continuing work are provided.

Accession For	
NTIS CR&AI	<input checked="" type="checkbox"/>
DTIC TAB	<input type="checkbox"/>
Unannounced	<input type="checkbox"/>
Justification	
By _____	
Distribution/	
Availability Codes	
Avail and/or Dist	Special
A	

Approved for public release; distribution unlimited.

Cerenkov Radiation

by

Ahmet Saglam  
Lieutenant Junior Grade, Turkish Navy  
B.S.E.E., Naval Postgraduate School, 1981

Submitted in partial fulfillment of the  
requirements for the degree of

MASTER OF SCIENCE IN PHYSICS

from the  
NAVAL POSTGRADUATE SCHOOL

December 1982

Author:

Ahmet

Approved by:

Fred R Bushuk Thesis Advisor

John R Neighbours Second Reader

J M Dyer Chairman, Department of Physics

William M Tolles Dean of Science and Engineering

### ABSTRACT

Cerenkov radiation is calculated for electron beams which exceed the velocity of radiation in a nondispersive dielectric medium. The electron beam is assumed to be bunched as emitted from a travelling wave accelerator, and the emission region is assumed to be finite. Predictions include (a) emission of harmonics of the bunch rate, (b) coherence of radiation at low frequencies, (c) smearing of the emission angle for finite emission regions, (d) explicit evaluation of power spectrum in terms of bunch dimensions. The results of theory are applied to microwave emission from fast electrons in air for different lengths of the air path. Problems encountered during the experiment are discussed and suggestions for continuing work are provided.

TABLE OF CONTENTS

I.	INTRODUCTION -----	9
II.	THEORY -----	10
A.	CALCULATION OF POYNTING VECTOR -----	10
B.	FOURIER COMPONENTS OF CURRENT -----	13
C.	VECTOR POTENTIAL -----	15
D.	RADIATED POWER -----	17
E.	RESULTS OF THEORY -----	22
III.	EXPERIMENTAL EQUIPMENT AND PROCEDURE -----	33
IV.	DISCUSSION -----	46
A.	EFFECTS OF REFLECTOR AND ANTENNA -----	46
B.	CONCLUSION -----	50
APPENDIX A:	DERIVATION OF CERENKOV RADIATION FOR A SINGLE PULSE OF CHARGE -----	52
APPENDIX B:	DERIVATION OF EQUATION 7 -----	57
APPENDIX C:	CALCULATIONS -----	59
APPENDIX D:	FORTRAN PROGRAM LISTINGS -----	65
LIST OF REFERENCES -----	69	
INITIAL DISTRIBUTION LIST -----	70	

### LIST OF FIGURES

1.	$I^2$ as a Function of $\theta$ ( $f = 8.57$ GHz) -----	20
2.	$I^2$ as a Function of $\theta$ ( $f = 14.28$ GHz) -----	21
3.	$dP/d\Omega$ as a Function of $\theta$ ( $f = 8.57$ GHz) -----	26
4.	$dP/d\Omega$ as a Function of $\theta$ ( $f = 14.28$ GHz) -----	27
5.	Total $dP/d\Omega$ as a Function of $\theta$ ( $N = 3,10$ ) -----	28
6.	Total $dP/d\Omega$ as a Function of $\theta$ ( $N = 5,10$ ) -----	29
7.	$dP/d\Omega$ as a Function of Frequency -----	31
8.	Cerenkov Angle as a Function of Frequency -----	32
9.	Air Cerenkov Experimental Setup 1 -----	34
10.	Signal Amplitude as a Function of Position (X Band, $L_1 = 89$ cm) -----	35
11.	Signal Amplitude as a Function of Position (X Band, $L_1 = 66$ cm) -----	36
12.	Signal Amplitude as a Function of Position (K Band, $L_1 = 89$ cm) -----	38
13.	Signal Amplitude as a Function of Position (K Band, $L_1 = 66$ cm) -----	39
14.	Signal Amplitude as a Function of Rotation Angle (X Band, $L_1 = 89$ cm) -----	40
15.	Signal Amplitude as a Function of Rotation Angle (X Band, $L_1 = 109$ cm) -----	41
16.	Signal Amplitude as a Function of Rotation Angle (K Band, $L_1 = 89$ cm) -----	42
17.	Signal Amplitude as a Function of Rotation Angle (K Band, $L_1 = 109$ cm) -----	43
18.	Air Cerenkov Experimental Setup 2 -----	45
19.	Air Cerenkov Experimental Setup 3 -----	48

20. Beam Current as a Function of Time -----	61
21. Relation Between Observed and Actual Beam Current -----	62

ACKNOWLEDGMENT

The author wishes to express his gratitude to Professor Fred R. Buskirk and Professor John R. Neighbours for their advice and guidance in all phases of this project.

Assistance of Mr. Don Snyder in the fabrication of the experimental setup and in the day-to-day operation and maintenance of the NPS LINAC is greatly appreciated.

Finally, the author wishes to thank his wife, Selma, for her understanding, patience and support throughout this work.

## I. INTRODUCTION

Cerenkov radiation is generated by a charged particle moving at greater than light speed in a particular medium. Because the distribution of intensity of Cerenkov radiation is proportional to the frequency, the radiated power at microwave frequencies would be low unless beams are intense and bunched so that coherent radiation by many electrons contributes.

Recent developments of electron accelerators for applications such as free electron lasers (FEL) have aimed toward high peak currents in bunches in contrast to nuclear and particle physics applications, where low peak but high average currents are desirable to avoid saturating detectors. The high peak currents in the new accelerators should yield enhanced Cerenkov radiation.

The intent of this experiment is to find Cerenkov radiation intensity and angle of emission in X Band and K Band regions.

## II. THEORY

### A. CALCULATION OF THE POYNTING VECTOR

In the following derivation, we consider the Cerenkov radiation produced in a dispersionless medium such as a gas or other dielectric, by a series of pulses of electrons such as are produced by a traveling wave electron accelerator (LINAC). The pulses or bunches are periodic, the total emission region is finite and the bunches have a finite size.

In determining the radiated power, procedure is to calculate the Poynting vector from fields which are in turn obtained from solutions of the wave equations for the potentials. Since the current and charge densities entering into the wave equations are expressed in Fourier form; the resulting fields and radiated power also have Fourier components. In the derivation  $\vec{r}$  is the coordinate at which the fields will be calculated,  $\vec{r}'$  is the coordinate of an element of the charge which produces the fields and  $\hat{n}$  is a unit vector in the direction of  $\vec{r}$ .

We assume that  $\vec{E}(\vec{r},t)$  and  $\vec{B}(\vec{r},t)$  have been expanded in a Fourier series, appropriate for the case where the source current is periodic. Then we have

$$\vec{E}(\vec{r},t) = \sum_{\omega=-\infty}^{\infty} e^{-i\omega t} \hat{\vec{E}}(\vec{r},\omega) \quad (1)$$

and a corresponding expansion for  $\vec{B}$ , where  $\omega$  is a discrete

variable and  $\vec{E}$  and  $\vec{B}$  are Fourier series coefficients. The Poynting vector  $\vec{S}$  is given by

$$\vec{S} = \frac{1}{\mu} \vec{E} \times \vec{B} \quad (2)$$

and it is easy to show that the average of  $\vec{S}$  in a direction given by a normal vector  $\hat{n}$  is

$$\frac{1}{T} \int_0^T \hat{n} \cdot \vec{S} dt = \frac{1}{\mu} \sum_{\omega=-\infty}^{\infty} \hat{n} \cdot \vec{E}(\vec{r}, \omega) \times \vec{B}(\vec{r}, \omega) \quad (3)$$

where  $T$  is an integer multiple of the period of the periodic current.

Letting  $c = (\mu \epsilon)^{-1/2}$  be the velocity of light in the medium, the wave equations for  $\vec{A}$ ,  $\phi$  and their solutions are,

$$(\nabla^2 - \frac{1}{c^2} \frac{\partial^2}{\partial t^2}) \vec{A}(\vec{r}, t) = \mu \vec{J}(\vec{r}, t) \quad (4)$$

$$(\nabla^2 - \frac{1}{c^2} \frac{\partial^2}{\partial t^2}) \phi(\vec{r}, t) = \frac{1}{\epsilon} \rho(\vec{r}, t)$$

$$\vec{A}(\vec{r}, t) = \mu \iiint D(\vec{r} - \vec{r}', t - t') \vec{J}(\vec{r}', t') d^3 r' dt' \quad (5)$$

$$\phi(\vec{r}, t) = \frac{1}{\epsilon} \iiint D(\vec{r} - \vec{r}', t - t') \rho(\vec{r}', t') d^3 r' dt'$$

where the Green's function  $D$  is given by

$$D(\vec{r}, t) = \frac{1}{4\pi r} \delta(t - r/c) \quad (6)$$

The vector potential  $\vec{A}(\vec{r}, t)$  also can be developed in a Fourier series expansion of a form similar to (1) with an expression for the Fourier series coefficients given by (Appendix B):

$$\vec{A}(\vec{r}, \omega) = \frac{1}{T} \int_0^T dt \vec{A}(\vec{r}, t) e^{i\omega t} \quad (7)$$

$$= \iiint d^3 r' \vec{J}(\vec{r}', \omega) \frac{1}{4\pi} \frac{1}{|\vec{r}-\vec{r}'|} e^{i\omega |\vec{r}-\vec{r}'|/c}$$

Now if we assume that the observer is far from the source so that  $|\vec{r}| \gg |\vec{r}'|$  for regions where the integrand in (7) is important we can let  $|\vec{r}-\vec{r}'| = r - \hat{n} \cdot \vec{r}'$  in the exponential and  $|\vec{r}-\vec{r}'| = r$  in the  $|\vec{r}-\vec{r}'|^{-1}$  factor in (7) obtaining (where  $n = \vec{r}/r$ )

$$\vec{A}(\vec{r}, \omega) = \frac{\omega}{4\pi r} e^{i\omega r/c} \iiint d^3 r' \vec{J}(\vec{r}', \omega) e^{-i\frac{\omega}{c} \hat{n} \cdot \vec{r}'} \quad (8)$$

The Fourier series coefficients of the fields are obtained from those for the vector potential (8) through the usual relations  $\vec{B} = \vec{\nabla} \times \vec{A}$  and  $\vec{E} = -\vec{\nabla}\phi - \frac{\partial \vec{A}}{\partial t}$ . Under the conditions leading to (8) the field Fourier coefficients are

$$\vec{B}(\vec{r}, \omega) = \frac{\omega}{c} \hat{n} \times \vec{A}(\vec{r}, \omega) \quad (9)$$

$$\vec{E}(\vec{r}, \omega) = -cn \times \vec{B}(\vec{r}, \omega) \quad (10)$$

The poynting vector can now be found by using (9) and (10) in expansions like (1) and then substituting in (2). However it is more convenient to deal with the frequency components of the radiated power by substituting (9) and (10) into the expression for the average radiated power (3).

$$\frac{1}{T} \int_0^T \hat{n} \cdot \vec{S} dt = \frac{1}{\mu} \sum_{\omega=-\infty}^{\infty} \frac{2}{c} |\hat{n} \times \vec{A}(\vec{r}, \omega)|^2 \quad (11)$$

#### B. FOURIER COMPONENTS OF THE CURRENT

The expression (7) for the Fourier components of the vector potential contains the Fourier components of the current density. Consequently it is necessary to examine the form of the current and its Fourier development. Assume the current is in the z direction and periodic. If the electrons move with velocity v, and we ignore for the moment the x and y variables, the charge or current functions should have the general form

$$f(z, t) = \sum_{k_z} e^{ik_z z} \sum_{\omega} e^{-i\omega t} f(k_z, \omega) \quad (12)$$

Under the condition of rigid motion,

$$f(z, t) = f_0(z - vt) \quad (13)$$

It is easy to show that

$$f(k_z, \omega) = \delta_{\omega, k_z v} f_0(k_z) \quad (14)$$

where

$$f_0(k_z) = \frac{1}{z} \int_0^z e^{-ik_z z} f_0(z) dz \quad (15)$$

Thus the restrictions of equation (13) reduce the two dimensional Fourier series of (12) to essentially a one dimensional series (14).

With (14) in mind, the current density associated with the electron beam from a linear accelerator should be periodic in both  $z$ ,  $t$ , with a Fourier series expansion but the  $x$  and  $y$  dependence should be represented by a Fourier integral form:

$$J_z(\vec{r}, t) = v_0(\vec{r}, t) = \frac{v}{2\pi} \int_{-\infty}^{\infty} dk_x \frac{1}{2\pi} \int_{-\infty}^{\infty} dk_y \cdot \sum_{k_z=-\infty}^{\infty} e^{i(\vec{k} \cdot \vec{r} - \omega \cdot t)} \rho_0(\vec{k}) \quad (16)$$

where the Fourier components of the charge density are

$$\rho_0(\vec{r}) = \int_{-\infty}^{\infty} dy \int_{-\infty}^{\infty} dy \frac{1}{z} \int_0^z dz e^{-ik \cdot \vec{r}} \rho_0(\vec{r}), \quad (17)$$

$\rho_0(\vec{r})$  is  $\rho(\vec{r}, t)$  evaluated at  $t = 0$  and  $\vec{J}$  is assumed to be in the  $z$  direction. Note in (16) that  $k_z$  and  $\omega$  are both discrete and from (14)  $\omega = k_z v$ .

### C. VECTOR POTENTIAL

The results of the previous section can be applied to the evaluation of the vector potential and in turn to the fields.

Let the infinite periodic pulse train be made finite, extending from  $z = -z'$  to  $z = +z'$ , so that  $2z'$  is the length of the path which generates radiation. Let  $\theta$  be the angle between  $\hat{n}$  and  $\vec{A}$ . Then the cross product in (11) can be written

$$\begin{aligned} |\hat{n} \times \vec{A}(\vec{r}, \omega)| &= \sin \theta \frac{\omega}{4\pi r} e^{i\omega r/c} \\ &\cdot \int_{-\infty}^{\infty} dx' \int_{-\infty}^{\infty} dy' \int_{-z'}^{z'} dz' e^{-i\frac{\omega}{c}\hat{n} \cdot \vec{r}'} \\ &\cdot \left(\frac{1}{2\pi}\right)^2 \int_{-\infty}^{\infty} dk_x \int_{-\infty}^{\infty} dk_y \\ &\cdot \sum_{k_z=-\infty}^{\infty} v_0(\vec{k}) \delta_{k_z} v_{\omega} e^{i\vec{k} \cdot \vec{r}'} \end{aligned} \quad (18)$$

But

$$\begin{aligned} &\int_{-\infty}^{\infty} dx' \int_{-\infty}^{\infty} dy' \int_{-z'}^{z'} dz' e^{i\vec{r}' \cdot (\vec{k} - \frac{\omega}{c}\hat{n})} \\ &= (2\pi)^2 \delta(k_x - n_x \frac{\omega}{c}) \delta(k_y - n_y \frac{\omega}{c}) I(z') \end{aligned} \quad (19)$$

where

$$I(z') = \int_{-z'}^{z'} dz' e^{i(k_z - n_z \frac{\omega}{c})} = \frac{2}{G} \sin Gz' \quad (20)$$

and

$$G = k_z - n_z \frac{\omega}{c} = \frac{\omega}{v} - n_z \frac{\omega}{c}$$

And thus the cross product term is

$$|\vec{n} \times \vec{A}(\vec{r}, \omega)| = \sin \theta \frac{\mu}{4\pi r} e^{i\omega r/c} v_{s_0} (\frac{n_x \omega}{c}, \frac{n_y \omega}{c}, \frac{\omega}{v}) I(z') \quad (21)$$

Note that  $\omega$  is a discrete variable but from (19), the continuous variables  $k_x$  and  $k_y$  become evaluated at discrete points.

Returning to (17), a more symmetric form may be obtained by assuming that  $s_0(\vec{r})$ , which is periodic in  $z$  with period  $Z$ , is actually zero between the pulses. Denoting by  $s'_0(\vec{r})$  the charge density of a single pulse, which is zero for  $z < 0$  and  $z > Z$  the integral on  $z$  can be written

$$\begin{aligned} \int_0^Z dz e^{-ik_z z} s_0(\vec{r}) &= \int_0^Z dz e^{-ik_z z} s'_0(\vec{r}) \\ &= \int_{-\infty}^{\infty} dz e^{-ik_z z} s'_0(\vec{r}) \end{aligned} \quad (22)$$

Then (17), the Fourier coefficient of the charge density, becomes

$$\rho_0(\vec{k}) = \frac{1}{Z} \iiint_{-\infty}^{\infty} d^3r e^{-i\vec{k} \cdot \vec{r}} \rho_0'(\vec{r}) = \frac{1}{Z} \rho_0'(\vec{k}) \quad (23)$$

where  $\rho_0'(\vec{k})$  is the three dimensional Fourier transform of the single pulse described by  $\rho_0'(\vec{r})$ . Substituting those expressions into (21) gives a final simple result for the cross product form:

$$|n \times \vec{A}(\vec{r}, \omega)| = \sin \theta \frac{n}{4\pi r} e^{i\omega r/c} \frac{v}{Z} \rho_0'(\vec{k}) I(z') \quad (24)$$

where

$$I(z') = \frac{2}{G} \sin Gz'$$

$$G = \frac{z}{v} - n_z \frac{\omega}{c} \quad (25)$$

$$\vec{k} = (n_x \cdot \omega/c, n_y \cdot \omega/c, \frac{\omega}{v})$$

The components of the Cerenkov  $\vec{E}$  and  $\vec{B}$  fields may now be found by substituting (24) in (9) and (10).

#### D. RADIATED POWER

The frequency components of the average radiated power are obtained by substituting (24) into (11). The negative frequency terms equal the corresponding positive frequency terms, yielding a factor of 2 when the summation range is changed. Multiplying by  $r^2$  converts to average power per unit solid angle,  $d\Omega/dk$ ,  $\propto 1/k^4$

$$\begin{aligned}\frac{dP}{d\Omega} &= r^2 \frac{1}{T} \int_0^T \hat{n} \cdot \vec{S} dt = \frac{2}{\mu} \sum_0^\infty \frac{\omega^2}{c} |\hat{n} \times \vec{A}(\vec{r}, \omega)|^2 \\ &= \sum_0^\infty W(\omega, \hat{n}),\end{aligned}\quad (26)$$

where  $\hat{n}$  is defined to be

$$W(\omega, \hat{n}) = \frac{2\mu}{(4\pi)^2} \frac{\omega^2}{c} \sin^2 \theta v^2 \frac{1}{z^2} |\rho'_0(\vec{k})|^2 I^2(z') \quad (27)$$

$\hat{n}$  is the power per unit solid angle radiated at the frequency  $\omega$ , which is a harmonic of the basic angular frequency  $\omega_0$  of the periodic pulse train.

To find  $P_\omega$ , the total power radiated at the frequency  $\omega$ ,  $W$  is multiplied by  $d\Omega$  and integrated over solid angle. Note that  $n_z = \cos \theta$ , and as  $\theta$  varies,  $G$  changes according to (25), with  $dG = -\frac{z}{c} dn_z$  so that

$$d\Omega = d\phi \frac{c}{\omega} dG \quad (28)$$

Nothing that the integral over  $\phi$  yields  $2\pi$ , we find the result for the total radiated power at the frequency  $\omega$  for all angles.

$$P_\omega = \frac{\mu}{4\pi} \frac{\omega^2}{c} \frac{v^2}{z^2} \int_{G'}^{G''} \sin^2 \theta |\rho'_0(\vec{k})|^2 I^2(z) \frac{c}{\omega} dG \quad (29)$$

The remaining integral over  $G$  may now be examined. This  $\sin^2 \theta$  and  $\rho'_0$  factors may often be slowly varying compared to

the  $I^2(z')$  factor, which is shown in Figure 1 for  $f = 8.57$  GHz [and in Figure 2] for  $f = 14.28$  GHz]. These two figures are the results of (25) which was solved by a Fortran computer program [Appendix (D.1)]. For large  $z'$ , the peak in  $I^2(z')$  becomes narrow, and if the integrand may be neglected outside the physical range  $G' < G < G''$

$$\int_{G'}^{G''} I^2(z') dG = \int_{-\infty}^{\infty} 4z'^2 \left( \frac{\sin^2 G z'}{G z'} \right) dG = 4\pi z' \quad (30)$$

Then, evaluating the  $\sin \theta$  factor and  $\rho'_0(\vec{k})$  at the point corresponding to  $G = 0$  (which is  $\cos \theta = n_z = \frac{c}{v}$ ) shows that  $\theta$  at the peak of  $I(z')$  is the usual Cerenkov angle  $\theta_c$ . We thus obtain for large  $z'$

$$P_\omega = \frac{u}{4\pi} \omega v^2 \sin^2 \theta_c |\rho'_0(\vec{k})|^2 \frac{4\pi z'}{z^2} \quad (31)$$

Now let  $2z'/z =$  ratio of the interaction length to pulse spacing =  $N$ , the number of pulses. Also  $z = \frac{2\pi v}{\omega_0}$  so that, in the large  $z'$  limit,

$$P_\omega = \frac{u}{4\pi} \omega \omega_0 v \sin^2 \theta_c |\rho'_0(\vec{k})|^2 N \quad (32)$$

To compare with usual formulations (32) is divided by  $Nv$  to obtain the energy loss per unit path length per pulse:

$$\frac{dE}{dx} \approx \frac{u}{4\pi} \omega \omega_0 \sin^2 \theta_c |\rho'_0(\vec{k})|^2 \quad (33)$$

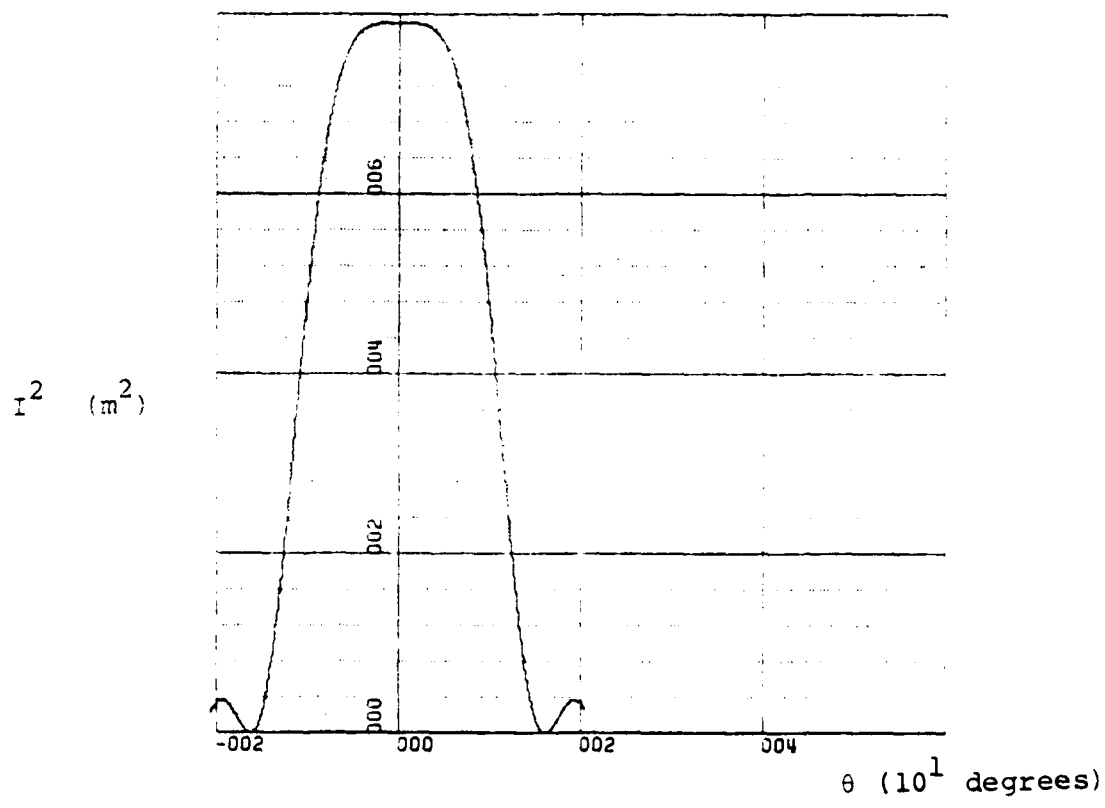


Figure 1.  $I^2$  as a Function of  $\theta$  ( $f = 8.57$  GHz)

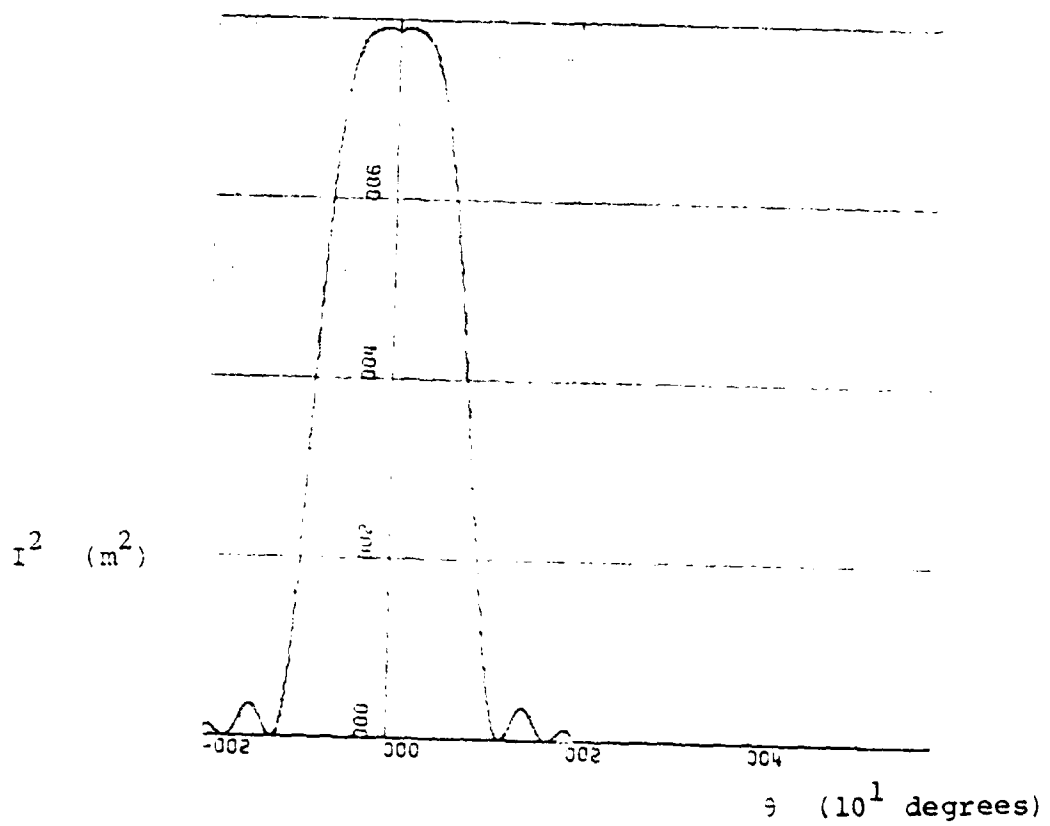


Figure 2.  $I^2$  as a Function of  $\theta$  ( $f = 14.28 \text{ GHz}$ )

If the pulse is in fact a point charge, the Fourier transform  $\rho_0'(\vec{k})$  reduces to  $q$ , the total charge per pulse and (33) is very similar to the usual Cerenkov energy loss formula, where for a single charge  $q$ , the radiation is continuous and the factor  $\omega\omega_0$  in (33) is replaced by  $\omega d\omega$ . In the present case the pulse train is periodic at angular frequency  $\omega_0$  and the radiation is emitted at the harmonic frequencies denoted by  $\omega$ .

#### E. RESULTS OF THEORY

Equation (29) and the approximate evaluation expressed as (32) form the main result. Some consequences will now be noted, and some calculations can be made.

##### 1. Effect of Pulse Size

The spatial distribution of the charge in the pulse appears in  $\rho_0'(\vec{k})$ , which is the Fourier transform of the charge distribution. One can easily see from (25) and Figure 1, the peak of  $I^2(z')$  occurs at  $G = 0$  or  $n_z = c/v$ . Thus at the peak,  $\omega/v = n_z \frac{\omega}{c}$  so that  $\vec{k}$ , the argument of  $\rho_0'(\vec{k})$ , is evaluated at

$$\vec{k} = \hat{n} \frac{\omega}{c} \quad (34)$$

We may also define a charge form factor  $F(\vec{k})$  as

$$\rho_0'(\vec{k}) = qF(\vec{k}) \quad (35)$$

The form factor  $\overset{\rightarrow}{F}(k)$  is identically one for a point charge, and for a finite distribution  $\overset{\rightarrow}{F}(k) = 1$  for  $k = 0$ .

Furthermore  $\overset{\rightarrow}{F}(k)$  must fall off as a function of  $\overset{\rightarrow}{k}$  near the origin if all the charge has the same sign. If the pulse were spherically symmetric,  $\overset{\rightarrow}{F}(k)$  would behave as elastic electron scattering form factors defined for nuclear charge distributions. In that case, the mean square radius  $\langle r^2 \rangle$  of the charge distribution is given by the behavior of  $\overset{\rightarrow}{F}(k)$  near the origin.

$$2Z\overset{\rightarrow}{F}(k) \rightarrow 1 - \langle r^2 \rangle \frac{k^2}{6} \quad (\text{spherical pulse}) \quad (36)$$

## 2. Smearing of the Cerenkov Angle

For a finite region over which emission is allowed, namely if  $2z'$  is finite, the function  $I^2(z')$ , appearing in the integral in (29), will have a finite width. Since the peak height is  $4z'^2$  and the area is (30), we can assign an effective width  $2\Gamma = \text{area}/\text{height} = \pi/z'$  or

$$\Gamma = \frac{\pi}{2z'} \quad (37)$$

Thus the radiation is emitted mainly near  $G = 0$  (which corresponds to  $\theta = \theta_c$ ) but in a range  $\Delta G = \pm\Gamma$ . But from (25),  $\Delta G = \frac{\omega}{c} \Delta n_z = \frac{\omega}{c} \Delta(\cos \theta)$  so that there is a range in  $\cos \theta$  over which emission occurs:

$$\int_{\cos \theta_c - \frac{\pi}{2z'}}^{\cos \theta_c + \frac{\pi}{2z'}} \frac{d\omega}{\omega} \quad (38)$$

Note that the finite angular width of the Cerenkov cone angle in (38) has the factor  $1/\omega$ , indicating that the higher harmonics are emitted in a sharper cone.

This result is shown in Table 1. Values are calculated by use of the same Fortran computer program as in Appendix (D1).

TABLE 1

Frequency (GHz)	$\theta_c^\circ$	$\theta^\circ$ $I^2_{\min}$	$J(\cos \theta)$
8.57	1.509	16.129	0.039
14.28	1.509	12.259	0.022
19.99	1.509	10.539	0.016
25.7	1.509	9.249	0.013
28.56	1.509	8.819	0.011
37.128	1.509	7.959	0.009
42.84	1.509	7.09	0.007

### C. BEHAVIOR AT HIGH FREQUENCIES RELATED TO PULSE PARAMETERS

To be specific let the charge distribution for a single pulse be given by Gaussian functions

$$\rho_0'(\vec{r}) = A \exp\left(-\frac{x^2}{a^2} - \frac{y^2}{a^2} - \frac{z^2}{b^2}\right) \quad (39)$$

Then  $F(\vec{k})$  may be found as

$$F(\vec{k}) = \exp\left(-\frac{k_x^2 a^2}{4} - \frac{k_y^2 a^2}{4} - \frac{k_z^2 b^2}{4}\right) \quad (40)$$

Beam pulse parameters could then be determine by measuring the Cerenkov radiation. For example, fast electrons from an accelerator in air will emit with a  $\theta_c$  of several degrees in which case  $k_x$  and  $k_y$  in (40) can be neglected, giving

$$F(\vec{k}) \approx \exp\left(-\frac{k_z^2 b^2}{4}\right) \approx \exp\left(-\frac{\omega^2}{c^2} \frac{b^2}{4}\right) \quad (41)$$

The average power emitted into a unit solid angle ( $dP/d\Omega$ ) as a function of angle ( $\theta$ ) is shown in Figure 3 for  $f = 8.57$  GHz [and in Figure 4 for  $f = 14.28$  GHz]. These two figures are the results of (26) which was solved by a second Fortran computer program [Appendix (D.2)].

Total power per unit solid angle as a function of angle ( $\alpha$ ) can be calculated by a third Fortran computer program [Appendix (D.3)] for many harmonic components in Figures 5 and 6. Figure 5 covers harmonics from 3 to 10, and Figure 6 covers harmonics from 5 to 10. For these two figures, the maximum power and the corresponding Cerenkov angle are shown in Table 2.

TABLE 2

$N_1$	$N_2$	$\sum_{N=N_1}^{N_2} (dP/d\Omega)_{\max}$	$\theta_c$
3	10	0.65 W	5°.99
5	10	0.55 W	5°.50

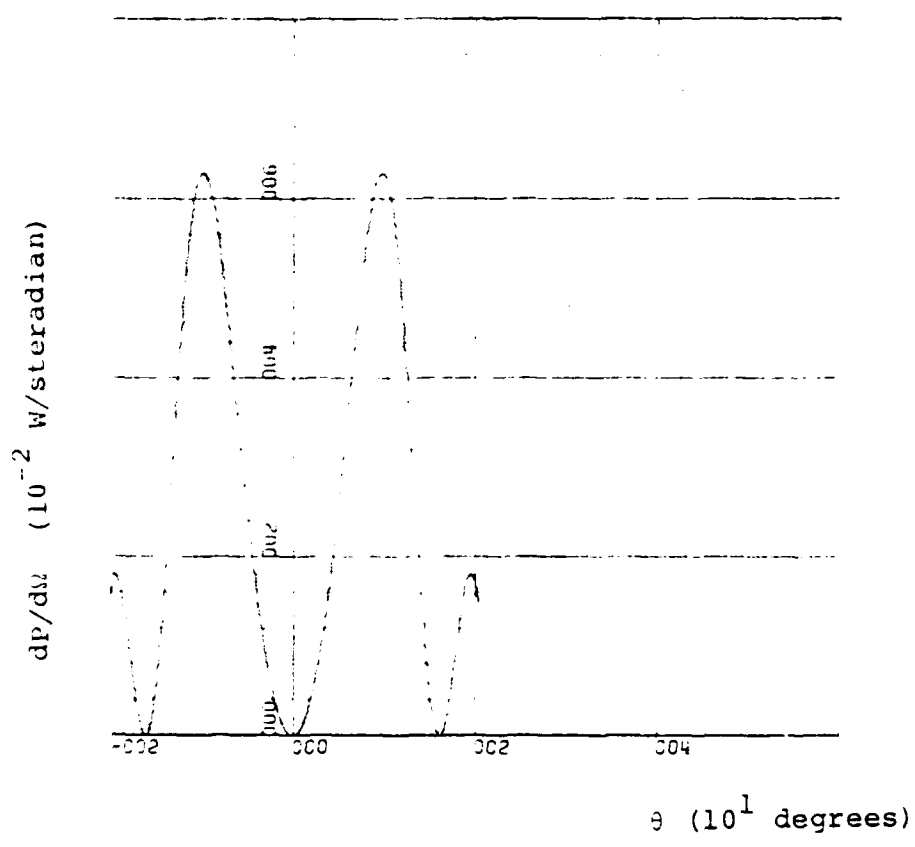


Figure 3.  $dP/d\Omega$  as a Function of  $\theta$  ( $f = 8.57$  GHz)

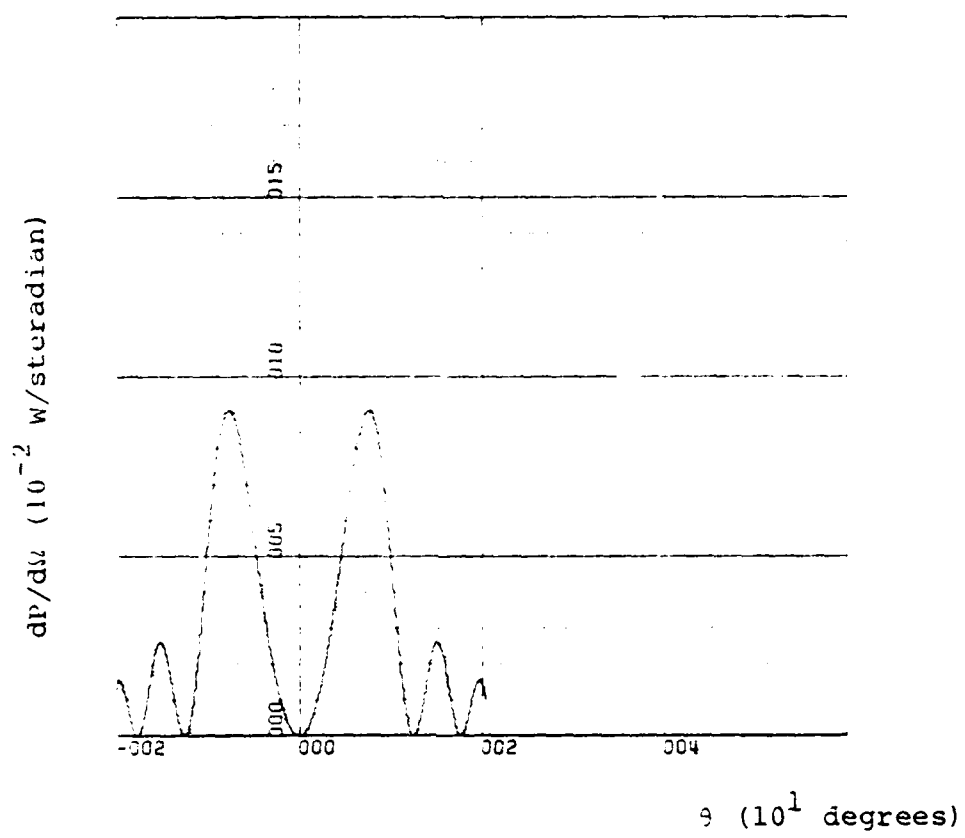


Figure 4.  $dP/d\Omega$  as a Function of  $\theta$  ( $f = 14.28 \text{ GHz}$ )

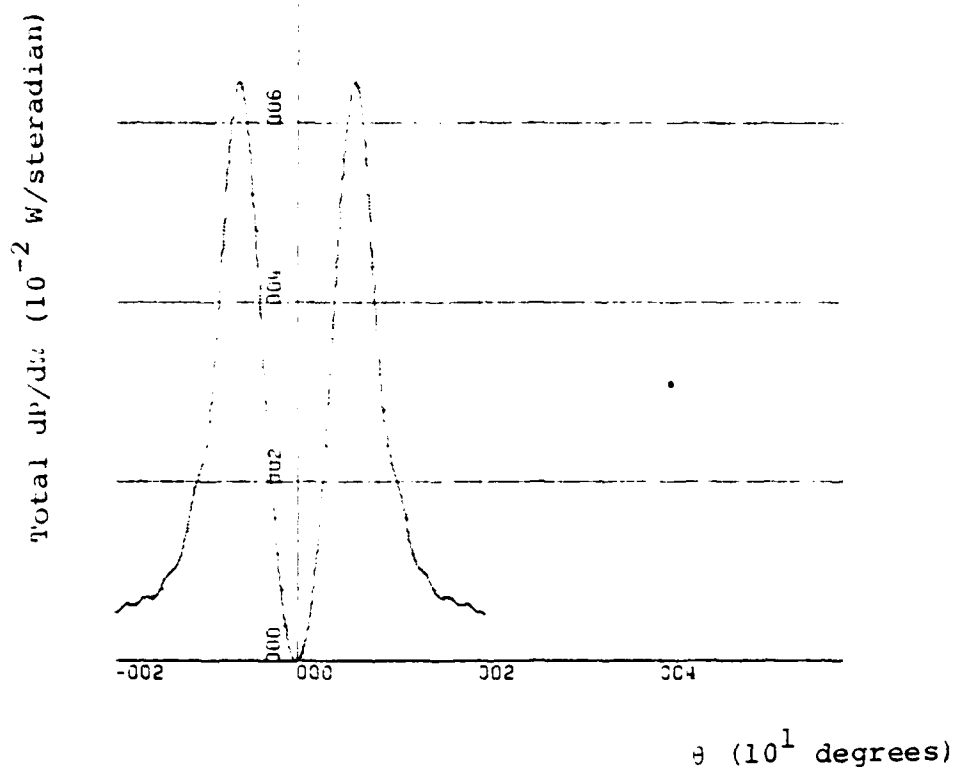


Figure 5. Total  $dP/d\Omega$  as a Function of  $\theta$  ( $N = 3,10$ )

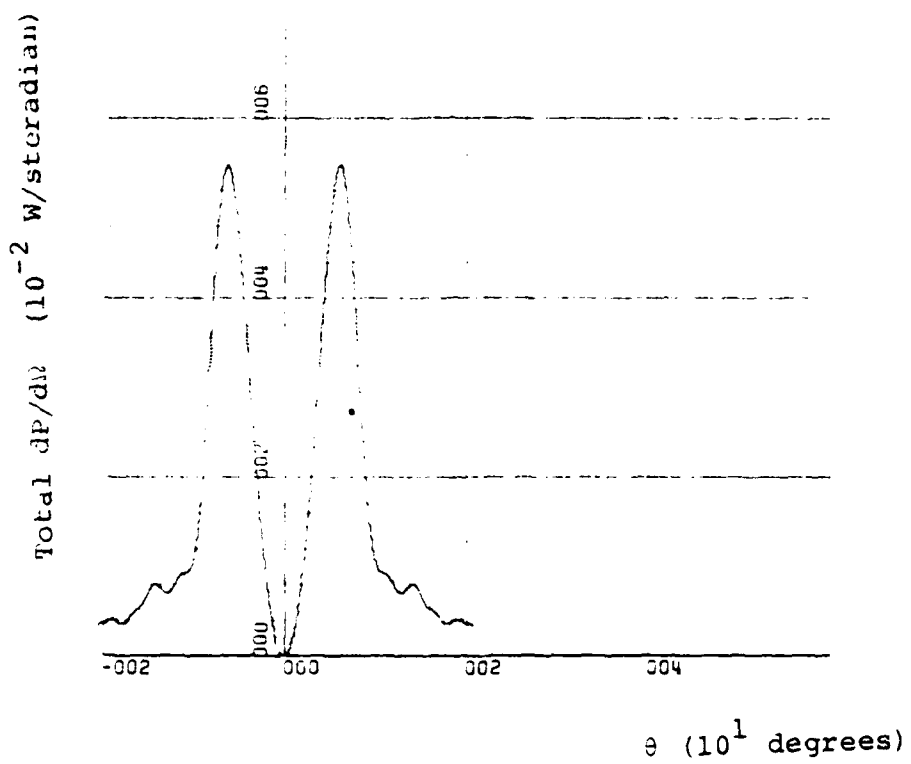


Figure 6. Total  $dP/d\Omega$  as a Function of  $\theta$  ( $N = 5, 10$ )

The behavior of  $dP/d\omega$  as a function of frequency is shown in Figure 7 (which is plotted with the help of the Fortran program in Appendix (D.2)). The linear rise at low frequencies followed by a fall off at higher frequencies, the peak occurring at

$$\omega_m = \frac{v}{b} \quad (42)$$

After inserting values of  $v$  and  $b$  into (42) (Appendix (C)),  $\omega_m$  is found to be  $126.86 \times 10^9$  rad/sec which corresponds to the same value as in Figure 7.

The Cerenkov angle is also plotted as a function of  $\omega$  in Figure 8 by use of the same Fortran program.

Furthermore, a different behavior would be expected at very high frequencies. The formulation from the beginning represents coherent radiation from all charges, not only from one pulse, but coherence from pulse to pulse.  $F(k)$  then describes interference of radiation emitted from different parts of the pulse, but note that expressions (29) and (32) will still be proportional to  $q^2 = n^2 e^2$  where  $n$  is the number of electrons in a pulse. Thus the  $n^2$  dependence of  $P_\omega$  indicates coherence. But above some high frequency  $\omega_1$  such that  $\omega_i/c = 2\pi/\lambda$ , where  $\lambda$  is the mean spacing of electrons in the cloud, the radiation should switch over to incoherent radiation from each charge and  $P_\omega$  should be proportional to  $n$ . The incoherent radiation should then rise again as a function of  $\omega$ .

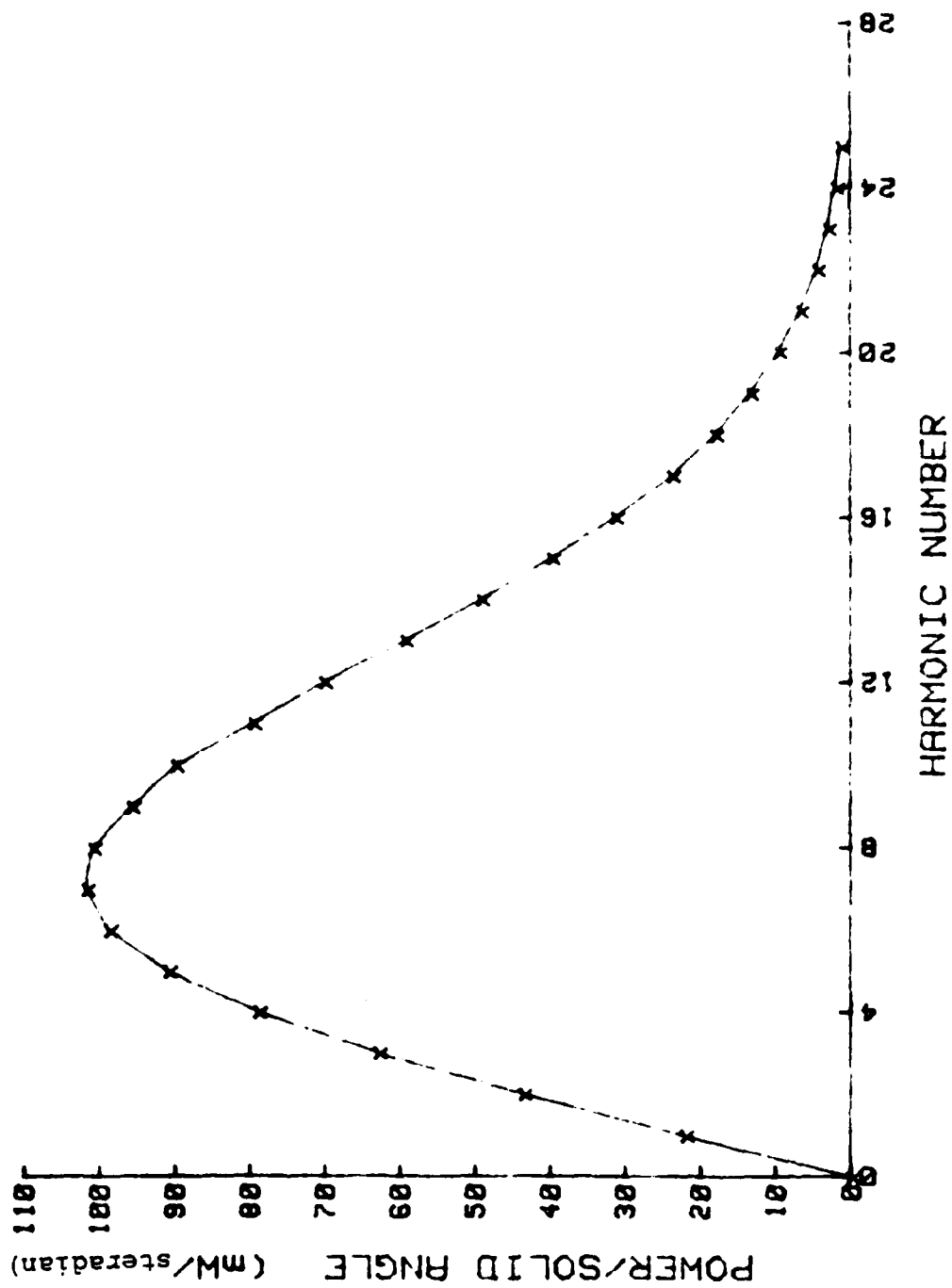


Figure 7.  $dP/dM$  as a Function of Frequency

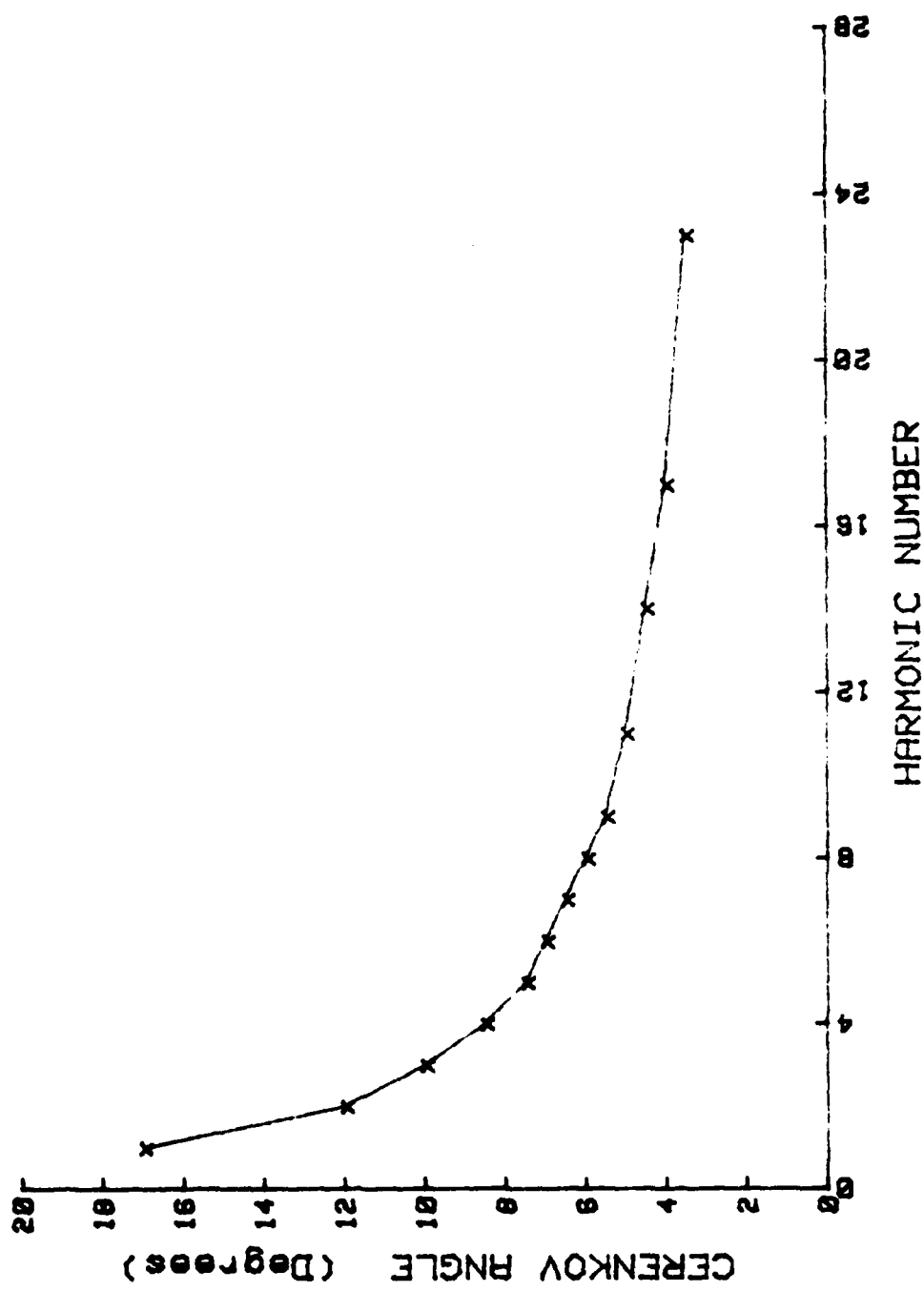


Figure 8. Cerenkov Angle as a Function of Frequency

### III. EXPERIMENTAL EQUIPMENT AND PROCEDURE

It was decided to find the frequency components of the average radiated power in the X Band (8.2-12.4 GHz) region. An experiment was designed to measure average radiated power as a function of angle.

The equipment arrangement is shown in Figure 9. The reflector used was a thin sheet of aluminum which would allow the passage of the electrons and reflect any EM radiation. X Band antenna, wave guide, detector (HP X424A) are mounted together. They were horizontally movable on this mount. Radiation was measured using a crystal detector connected to an oscilloscope (Tektronix 475 A, 200 MHz).

Experiments were made for air paths ( $L_1$ ) = 66 cm and 89 cm, and repeated in different days for many times. Results changed day by day depending upon beam current. When the beam current increased, the observed signal also increased. Figures 10 and 11 show the experimental results for Beam current equals  $2 \times 10^{-8}$  Amps.

Cerenkov angles were calculated by help of Figures 9 and 10 (or Figures 9 and 11).

From Figure 9, one can show that

$$\tan \theta_C = \frac{x}{2(L_2 + L_1/2)} \quad (43)$$

where:

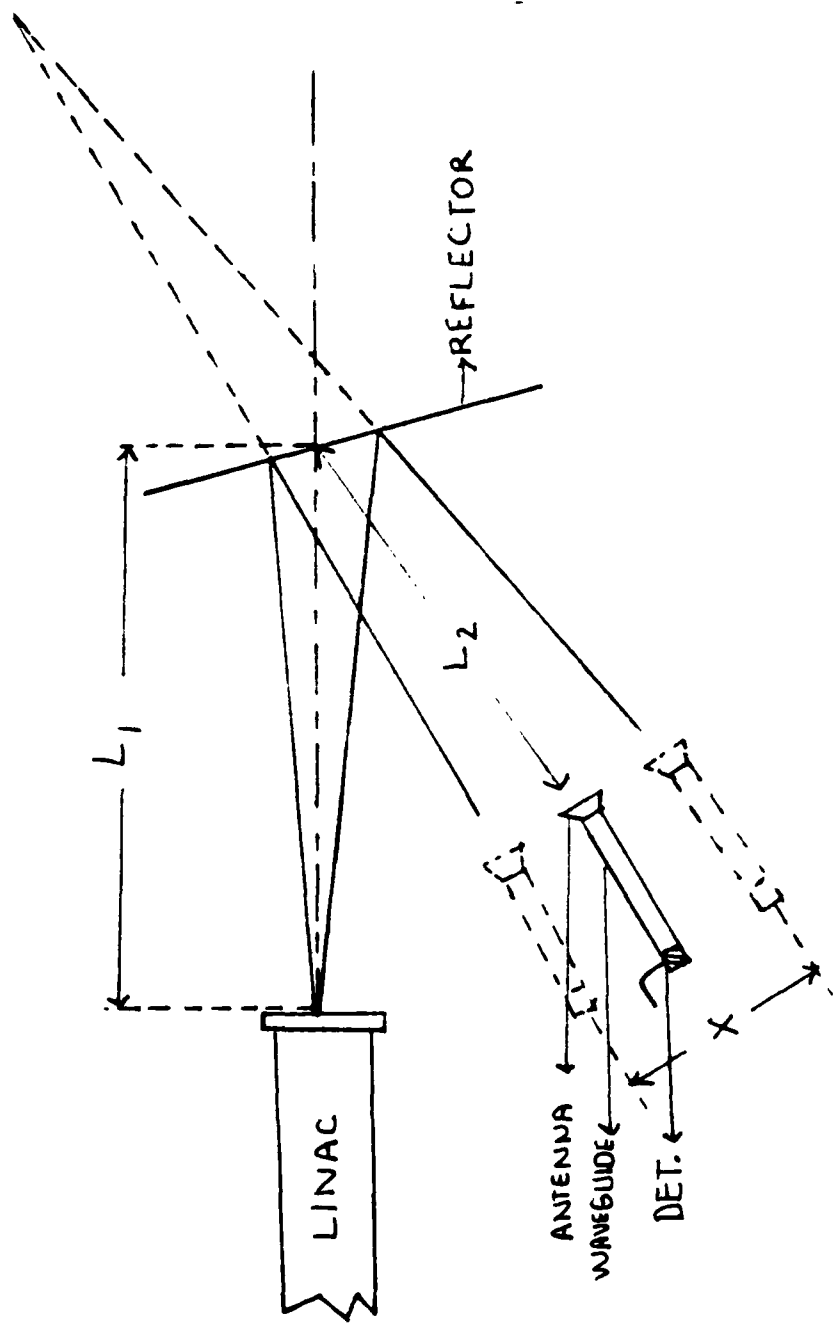


Figure 9. Air Cerenkov Experimental Setup 1

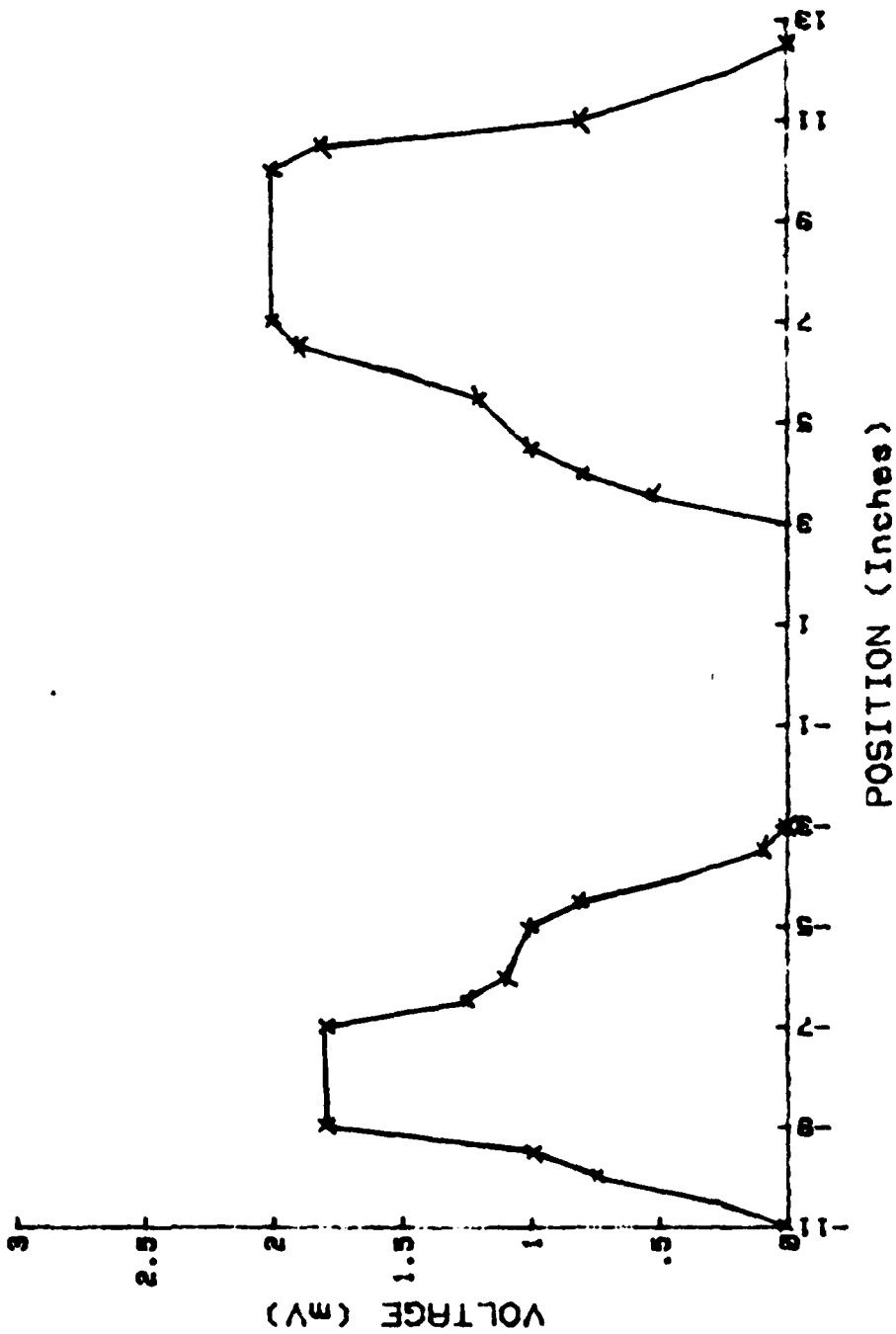


Figure 10. Signal Amplitude as a function of Position  
(X Band,  $L_1 = 89$  cm)

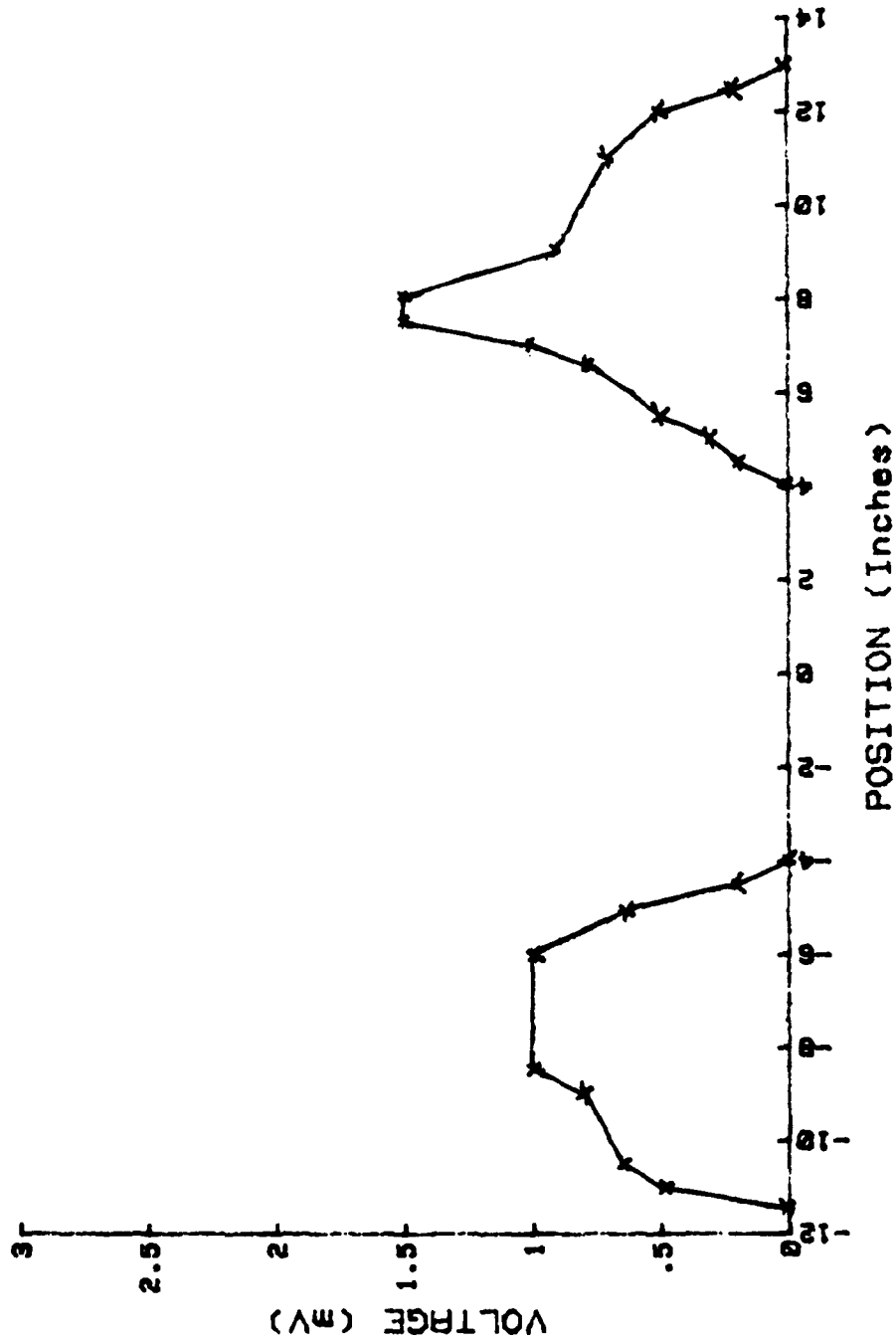


Figure 11. Signal Amplitude as a Function of Position  
(X Band,  $L_1 = 66$  cm)

$x$  = Distance between two maximum signal positions;

$L_1$  = Distance between LINAC and reflector (air path length);

$L_2$  = Distance between reflector and antenna.

Later experiments were conducted in the K Band region for the same air path lengths ( $L_1 = 66$  and  $89$  cm). Figures 12 and 13 show the experiment results for Beam current =  $2 \times 10^{-8}$ . Cerenkov angles were calculated for these four experiments. The results are shown in Table 3.

TABLE 3

$\theta_c^{\circ}$ (XB)	$\theta_c^{\circ}$ (KB)	$L_1$ (cm)	$L_2$ (cm)
8.21	5.94	89	99
9.13	6.97	66	86

To check the correctness of the measurements, another experiment was set up. The equipment arrangement was the same as before except this time the reflector was rotatable (a different, bigger aluminum thin sheet was used) and the antenna was at a fixed position. The experiment was repeated for two different air path lengths. Rotation angles ( $\alpha$ ) of three reflector versus signal voltages are plotted in Figures 14, 15, 16 and 17.

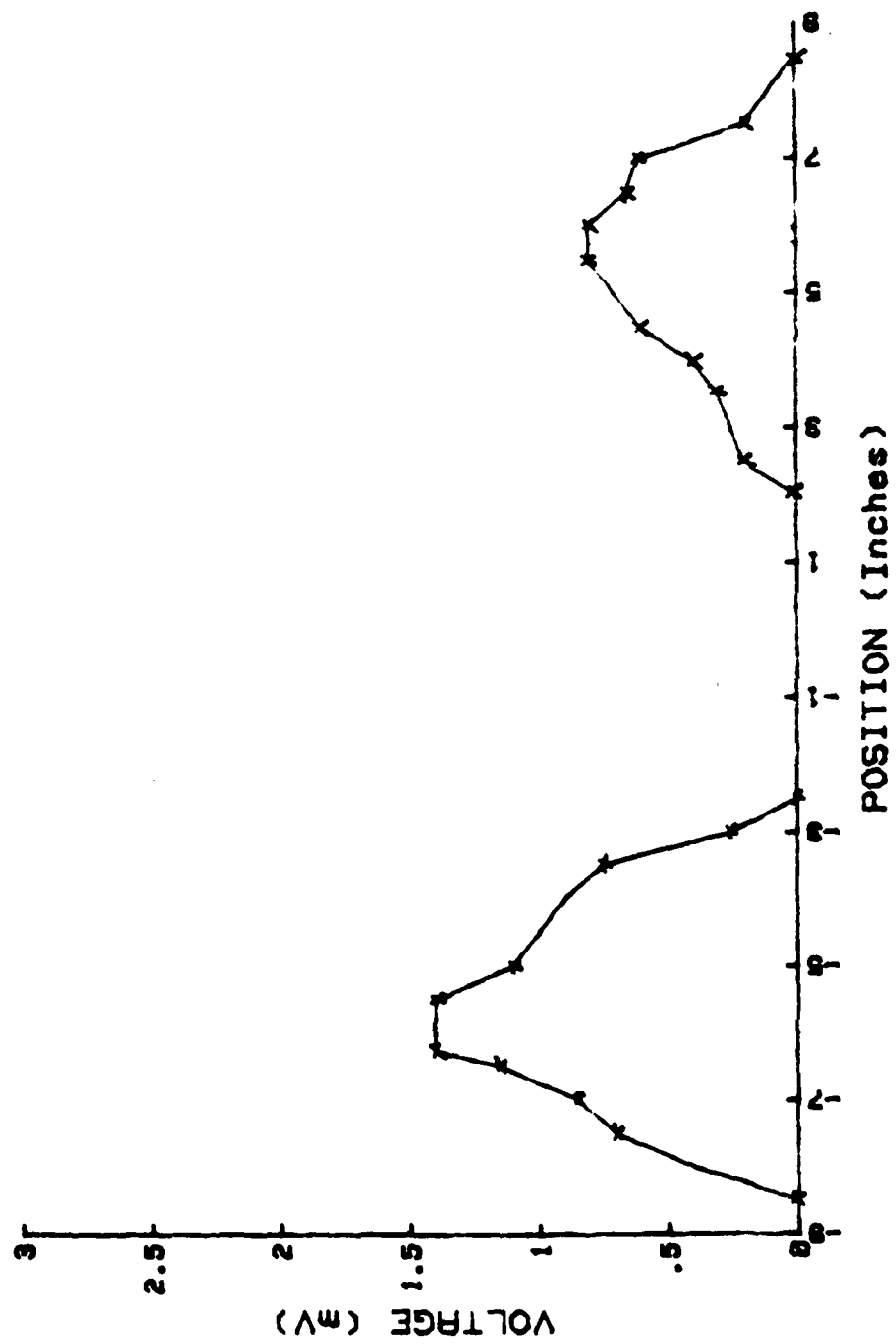


Figure 12. Signal Amplitude as a Function of Position  
(K Band,  $L_1$  - 89 cm)

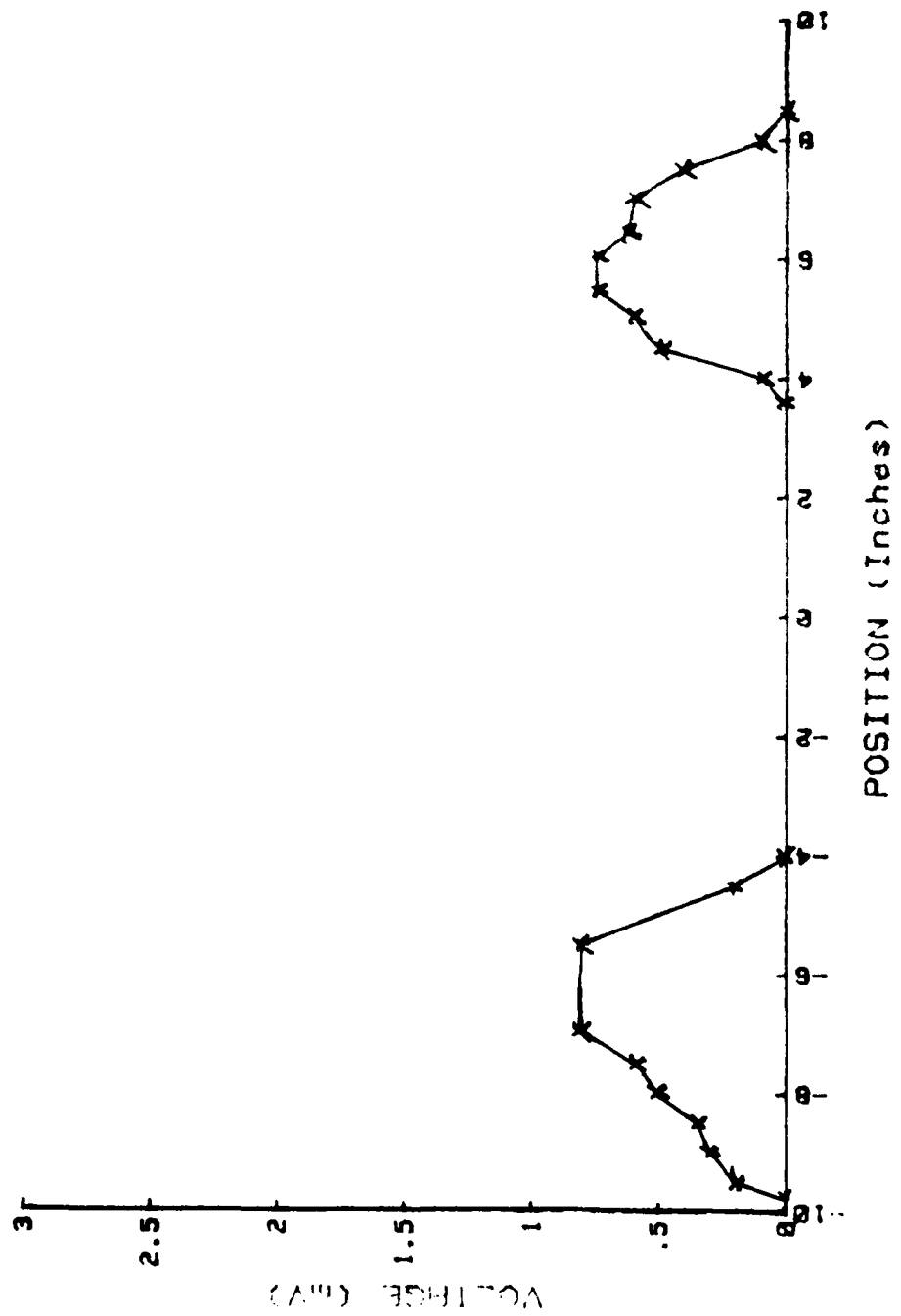


Figure 13. Signal Amplitude as a function of Position  
(K Band,  $I_1 = 66$  cm)  
(L Band,  $I_1 = 100$  cm)

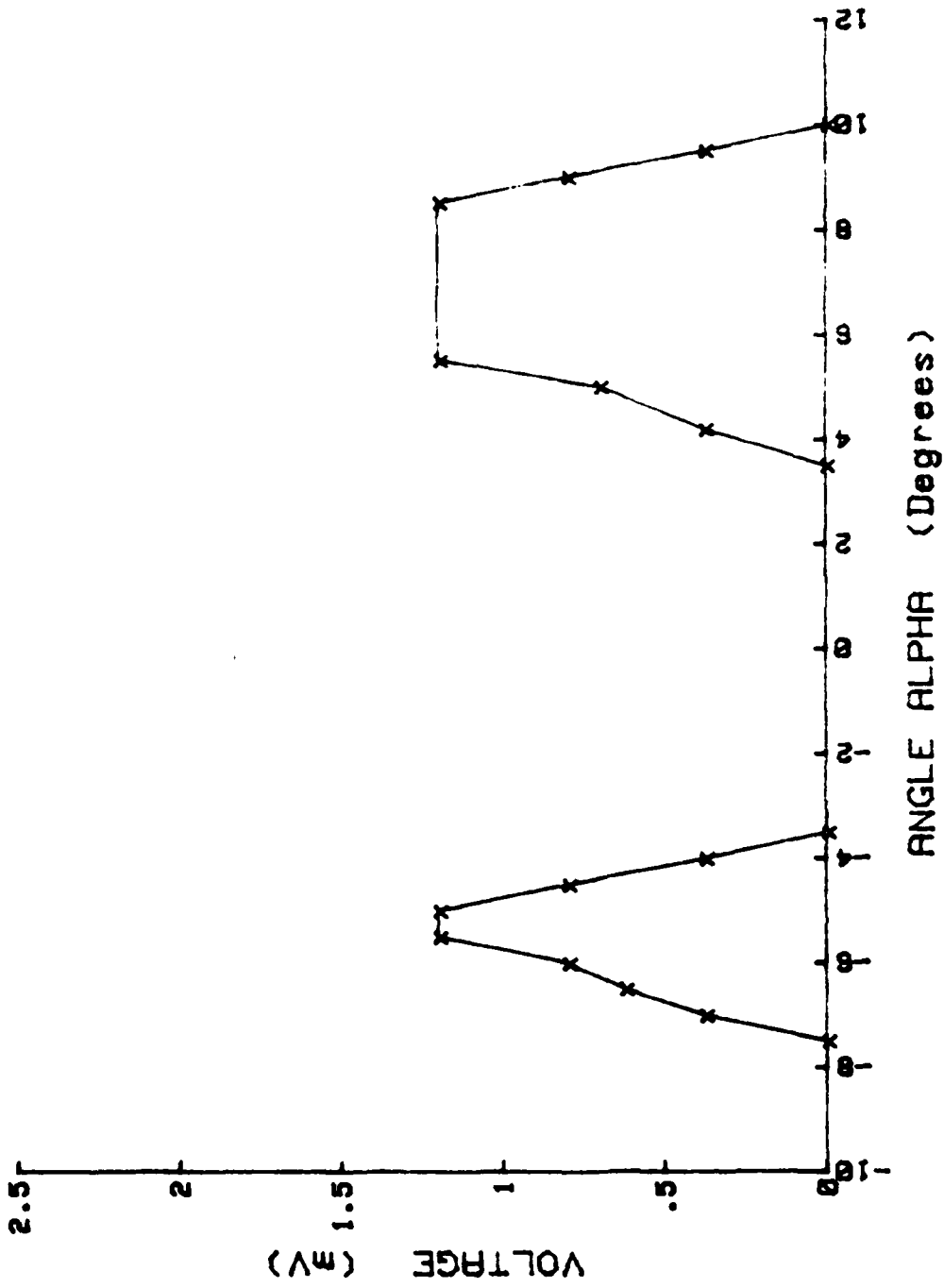


Figure 14. Signal Amplitude as a Function of Rotation Angle (X Band,  $b_1 = 89$  cm)

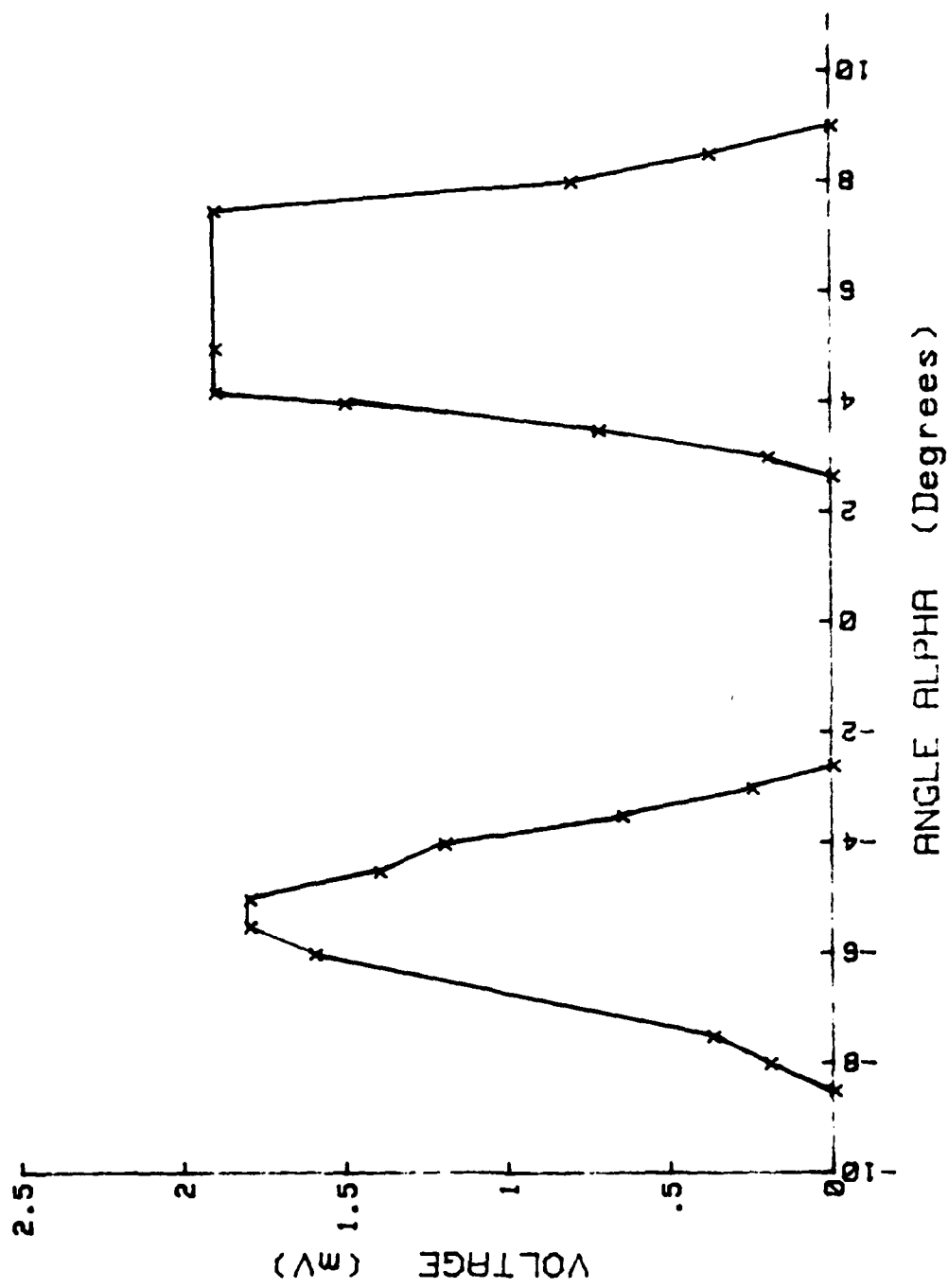


Figure 15. Signal Amplitude as a Function of Rotation Angle (X band,  $t_1 = 109$  cm)

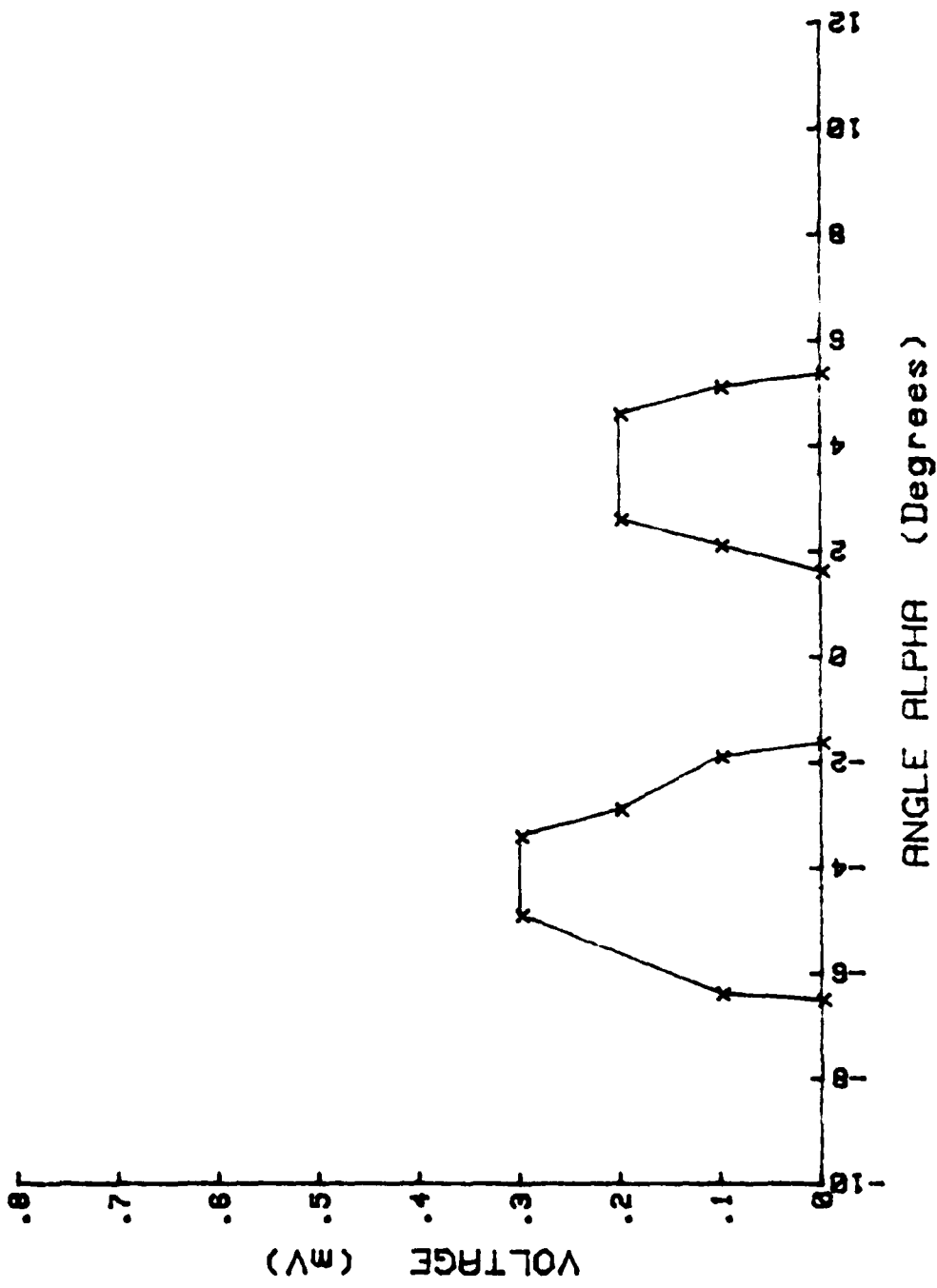


Figure 16. Signal Amplitude as a Function of Rotation Angle (K Band,  $L_1 = 89$  cm)

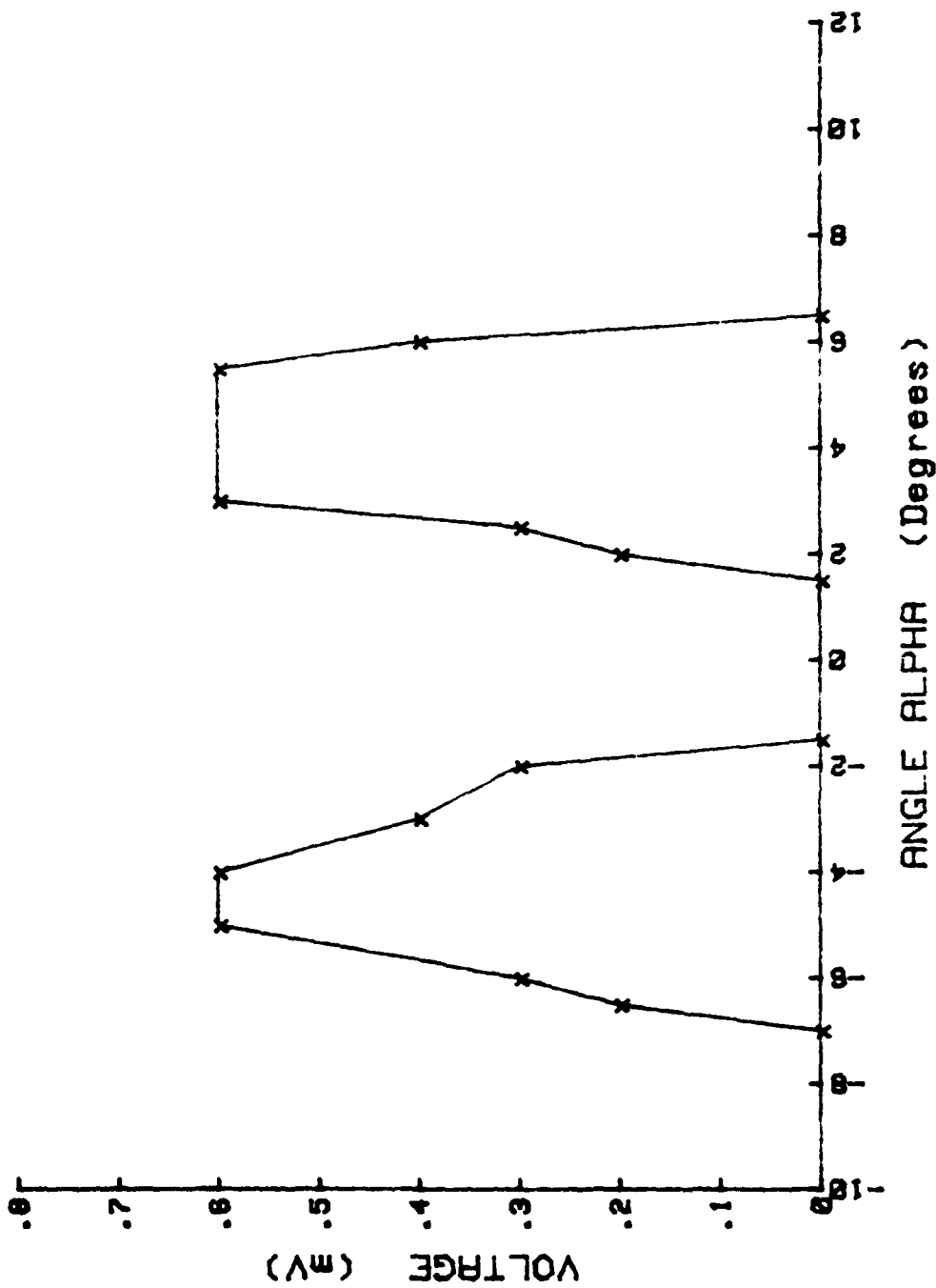


Figure 17. Signal Amplitude as a Function of Rotation Angle (K Band,  $L_1 = 109$  cm)

The relationship between  $\theta$  and  $\theta_c$  can be found from  
Figure 18. For small values of  $2\alpha$  and  $2\theta_c$

$$2\theta_c \sim \frac{s}{\frac{L_1}{2} + L_2} \text{ rad} \quad (44)$$

$$2\alpha \sim \frac{s}{L_1} \text{ rad} \quad (45)$$

From (44) and (45),

$$\theta_c = \alpha \frac{L_2}{L_2 + (L_1/2)} \quad (46)$$

where  $\alpha$  is the rotation angle of reflector between two maximum signal positions.

Cerenkov angles were calculated for various  $L_1$  values. Results are shown in Table 4.

TABLE 4

$L_1$ (cm)	$L_2$ (cm)	$\alpha^\circ$	$\theta_c^\circ$ (XB)	$\theta_c^\circ$ (KB)
66	86		No Signal	Observed
89	99	12	8.28	6.04
109	114	11	7.44	5.35

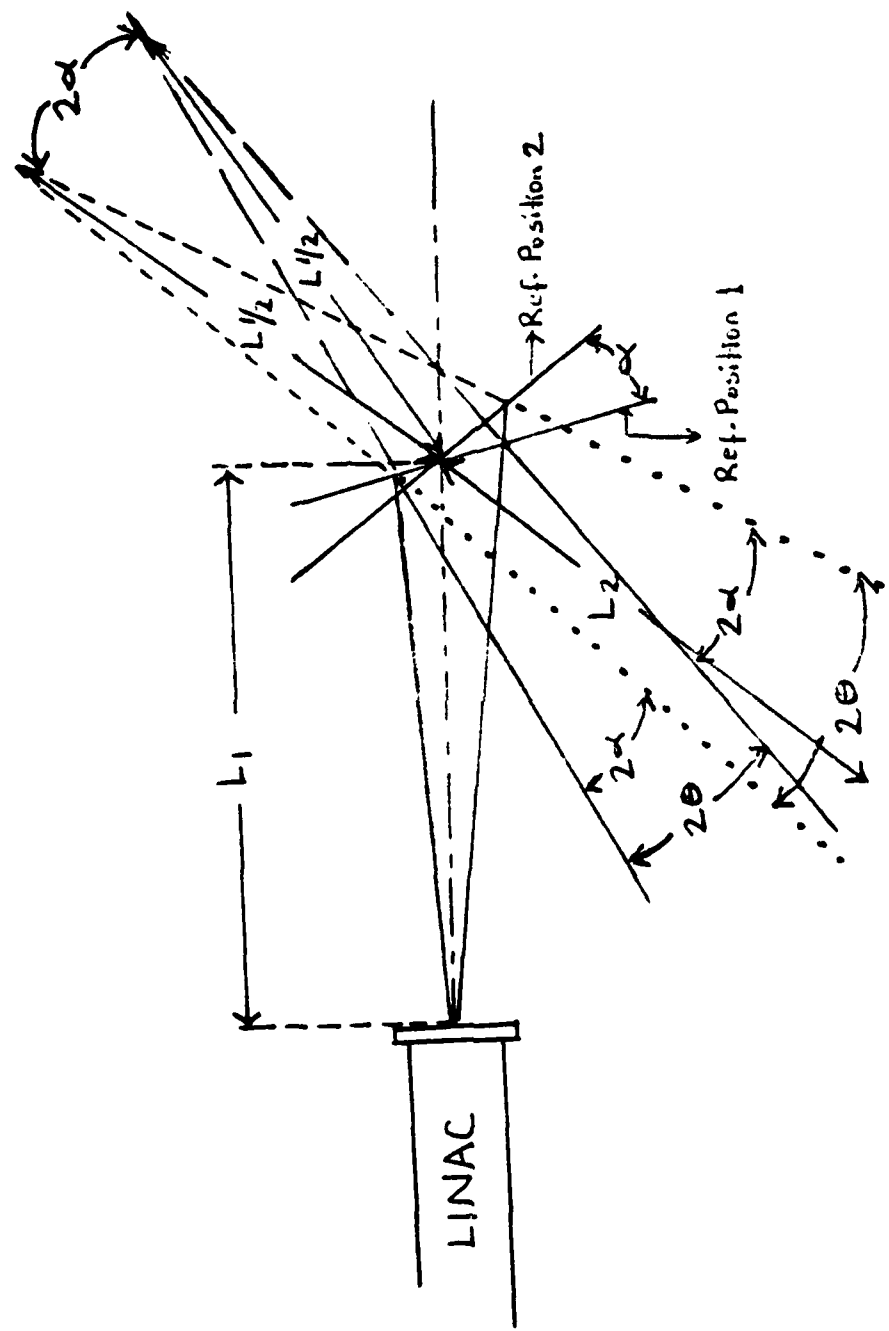


Figure 18. Air Cerenkov Experimental Setup 2

#### IV. DISCUSSION

##### A. EFFECTS OF REFLECTOR AND ANTENNA

In all experiments, the same X Band detector was used. Table 5 shows experimental values of  $\theta_c^\circ$  and  $dP/d\Omega$  assuming the X Band detector is performing in its Square Law region where the sensitivity is  $400 \mu V/\mu W$  [Ref. 1].

TABLE 5

	$\theta_c^\circ$	voltage (mV)	power (mW)
X Band ( $L_1 = 66 \text{ cm}$ )	9.13	1.5	$3.75 \times 10^{-3}$
X Band ( $L_1 = 89 \text{ cm}$ )	8.208	2	$5 \times 10^{-3}$
K Band ( $L_1 = 66 \text{ cm}$ )	6.67	0.8	$2 \times 10^{-3}$
K Band ( $L_1 = 89 \text{ cm}$ )	5.94	1.4	$3.5 \times 10^{-3}$

To make a comparison between experimental and theoretical results,  $L_1 = 89 \text{ cm}$  and  $\theta_c^\circ = 8.2$  were chosen from experimental data; and for these values [ $dP/d\Omega$ ] was calculated using the second Fortran program (Appendix C.2). The results are shown in Table 6.

Although antenna gains weren't included in calculations of theoretical values, as seen from Tables 5 and 6, experimental values are much smaller than theoretical ones. The reasons for this can be:

- a. Aluminum thin sheet is not an excellent reflector.

TABLE 6

$N_1$	$N_2$	$\sum_{N=N_1}^{N_2} dP/d\Omega$ (mW/steradian)	$\sum_{N=N_1}^{N_2} P$ (mW)
3	4	.135	$9.45 \times 10^{-2}$
3	5	.223	$15.61 \times 10^{-2}$
3	6	.308	$21.56 \times 10^{-2}$
3	7	.377	$26.39 \times 10^{-2}$
3	8	.424	$29.68 \times 10^{-2}$
3	9	.451	$31.57 \times 10^{-2}$
3	10	.461	$32.27 \times 10^{-2}$

b. Antenna responsivity is decreasing when distance between radiation source and antenna increased ( $L = L_1 + L_2$ ).

To check these conditions, another experiment was conducted for various  $L$  values with a setup as shown in Figure 19.

The results are shown in Table 7.

TABLE 7

	<u><math>L</math> (cm)</u>	<u>voltage (mV)</u>	<u>power (mW)</u>
X Band	80	130	$3.25 \times 10^{-1}$
X Band	160	20	$0.5 \times 10^{-1}$
K Band	74	20	$0.5 \times 10^{-1}$
K Band	151	18	$0.45 \times 10^{-1}$

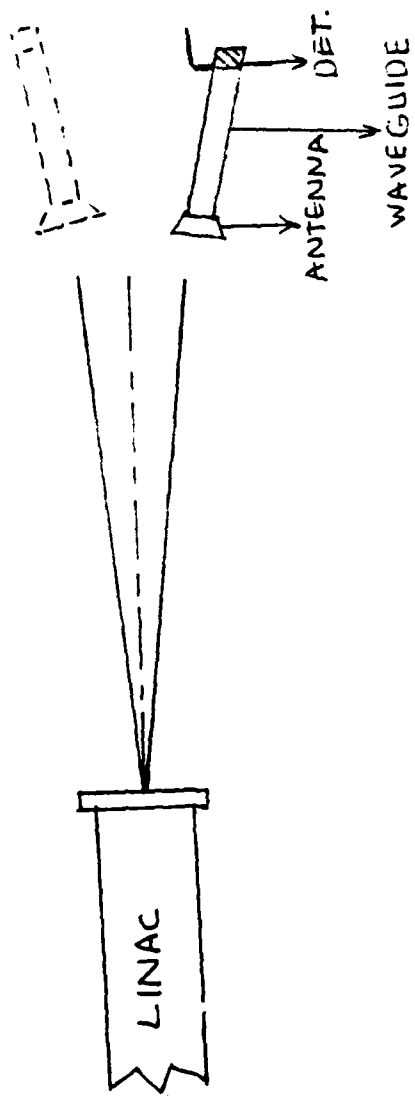


Figure 19. Air Cerenkov Experimental Setup 3

In this experiment some part of the observed signal may be caused by near field radiation, though, the results now seem more comparable with theoretical results and very close to  $\sum_{N=3}^{10} P_N$ .

To be able to make exact comparisons between experimental and theoretical values, antenna gains were found for these harmonics of the LINAC [Ref. 2].

Calculated values are shown in Table 8.

TABLE 8

Freq. (GHz)	Ant. Gain (X Band)	Ant. Gain (K Band)
8.57	11.67	---
11.42	20.31	---
14.28	30.64	71.28
17.14	42.46	90.34
19.99	55.08	105.55
22.85	68.67	116.66
25.70	81.72	122.22
28.56	94.58	122.98

For  $L_1 = 89$  cm, the result of the experiment was  $\gamma_c = 8.2$  (from Table 1). To make a comparison between experimental and theoretical values, theoretical value of average power emitted into a unit solid angle is calculated for some harmonics of the LINAC by use of the Fortran program in [Appendix (D.2)]. ( $\text{thus } \gamma_c = 8.2$ )

The results are shown in Table 9.

TABLE 9

N	$dP/d\Omega$ (mW/steradian)	$\text{Gain}_{XB}$ (mW/steradian)	$dP/d\Omega$ (mW/steradian)	$\text{Gain}_{KB}$ (mW/steradian)
3	$5.76 \times 10^{-2}$	.67	---	---
4	$5.62 \times 10^{-2}$	1.14	---	---
5	$8.83 \times 10^{-2}$	2.72	6.33	
6	$8.49 \times 10^{-2}$	3.60	7.67	
7	$6.9 \times 10^{-2}$	3.80	7.27	
8	$4.7 \times 10^{-2}$	3.23	5.48	
9	$2.6 \times 10^{-2}$	2.12	3.18	
10	$1.03 \times 10^{-2}$	0.97	1.27	

As seen from Tables 7 and 9, although the experimental values include more than one harmonic, the theoretical values are bigger than the experimental ones.

#### B. CONCLUSION

Although in these experiments only a very small signal was observed, all results indicated that the higher harmonics are emitter in a sharper cone. Nevertheless, some refinements remain to be done. Some specific suggestions are given below.

##### 1. Antenna Sensitivity

Antenna sensitivity has to be measured as a function of frequency and distance.

## 2. Detector Sensitivity

In the K Band region, a K Band detector should be used. The sensitivity of the detectors should be tested.

## 3. Coupling a Band Pass Filter to Detector

In the experiments, the X Band and K Band wave guides have certain lower end cutoff frequencies, but no upper end cutoff frequencies. If the experiments are conducted using a band pass filter (having constant response in its band), the effectiveness of measurements will be increased.

## 4. Noise Effect

The experimental area was very noisy. It affected the observed signals too much. Noise can be partially decreased by putting a detector into a thin aluminum box, which would decrease the electric field noise pickup. However, the magnetic field noise associated with the LINAC Klystrons is more difficult to shield.

## APPENDIX A

### DERIVATION OF CERENKOV RADIATION FOR A SINGLE PULSE OF CHARGE

Let the pulse be described by

$$\rho'(\vec{r}, t) = \rho'_0(\vec{r} - \vec{v}t) \quad (\text{A1})$$

Both  $k_z$  and  $\omega$  are continuous variables in this case;  $\vec{v}$  is again along the  $z$  axis. If we expand in terms of a four dimensional Fourier integral,

$$\rho'(\vec{r}, t) = (1/(2\pi)^4) e^{i(\omega t - \vec{k} \cdot \vec{r})} \tilde{\rho}'(\vec{k}, \omega) d^3 k d\omega \quad (\text{A2})$$

It may be shown that the condition (A1) gives:

$$\tilde{\rho}'(\vec{k}, \omega) = 2\pi \delta(\omega - k_z v) \rho'_0(\vec{k}) \quad (\text{A3})$$

where  $\tilde{\rho}'_0(\vec{k})$  is the three dimensional spatial transform of  $\rho'(\vec{r}, t)$  evaluated at  $t = 0$ . All the fields have Fourier integrals rather than Fourier series expansions and the energy radiated per unit solid angle becomes

$$\begin{aligned} r^2 \int_{-\infty}^{\infty} dt \hat{n} \cdot \hat{s} &= \frac{1}{2\pi} \left( \frac{1}{4\pi} \right)^2 \frac{u}{c} \int_{-\infty}^{\infty} d\omega \omega^2 \\ &\cdot \left| \iiint d^3 r' dt' e^{i\frac{\omega}{c}(ct' - \hat{n} \cdot \vec{r}')} \hat{n}_x \hat{j}(\vec{r}', t') \right|^2 \\ &= \int_0^{\infty} \omega \omega(\omega, n) d\omega \quad (\text{A4}) \end{aligned}$$

The integrand is a symmetric function of  $\omega$  so that

$$\begin{aligned} W(\omega, \hat{n}) &= \frac{1}{16\pi^3} \frac{\mu}{c} \omega^2 \iiint d^3 r' dt' e^{i\omega(t' - \hat{n} \cdot \vec{r}'/c)} \hat{n}_x \hat{J}(\vec{r}', t') \\ &= \frac{1}{16\pi^3} \frac{\mu}{c} \omega^2 (\hat{n}_x \hat{v})^2 \quad (A5) \end{aligned}$$

where

$$u = \iiint d^3 r' dt' e^{i(\omega t' - \hat{n} \cdot \vec{r}'/c)} \hat{J}(\vec{r}', t') \quad (A6)$$

Now we may write  $\hat{J}(\vec{r}', t')$  in a Fourier integral representation,

$$\hat{J}(\vec{r}', t') = \frac{1}{(2\pi)^3} \iiint d^3 k' d\omega' \delta'(\vec{k}', \omega') e^{-i(\omega' t' - \vec{k}' \cdot \vec{r}')} \quad (A7)$$

Inserting (A3) into (A7) and the result into (A6), the integral over  $d^3 k'$  involves only exponentials and yields  $(2\pi)^3 \delta^3(\vec{k}' - \hat{\omega n}/c)$ , so that (A6) becomes

$$u = \int dt' \iiint d^3 k' d\omega' e^{i(\omega - \omega') t'} \delta^3(\vec{k}' - \hat{\omega n}/c) \delta(\omega' - \vec{k}' \cdot \hat{v}) \hat{J}_0(\vec{k}')$$

Now the integral over  $\omega'$  may be done; because of the  $\delta$  function,  $\omega'$  is evaluated at  $\vec{k}' \cdot \hat{v}$ .

$$u = \int dt' \iiint d^3 k' e^{i(\omega - \vec{k}' \cdot \hat{v}) t'} \delta^3(\vec{k}' - \hat{\omega n}/c) \hat{J}_0(\vec{k}')$$

Now do the integrals over  $k'_x$ ,  $k'_y$  and  $k'_z$ , noting that  $k'_z$  appears in the exponential, but  $k'_x$  and  $k'_y$  do not,

$$M = \int dt e^{i\omega t} e^{-i\omega t' n_z v/c} \rho_0'(\omega n_x/c, \omega n_y/c, \omega n_z/c)$$

This may be written as

$$M = \int dt e^{i\omega t} \hat{\rho}_0'(\hat{n}\omega/c) \quad (\text{A8})$$

where

$$\hat{H} = 1 - n_z v/c \quad (\text{A9})$$

If we let the time interval be finite, from  $-T$  to  $+T$ , the integral is easily done:

$$M = \frac{2}{\omega} \sin \omega HT \hat{\rho}_0'(\hat{n}\omega/c) \quad (\text{A10})$$

$$M^2 = 4T^2 \frac{\sin^2 \omega HT}{2} |\hat{\rho}_0'(\hat{n}\omega/c)|^2 \quad (\text{A11})$$

This result, equation (A11) may be inserted in (A5) for  $\omega$ . The factor  $\hat{n}_x \hat{v}$  is just  $\sin \theta$  where  $\theta$  is the angle between the radiation and the beam axis.

$$W(\omega, n) = \frac{1}{16\pi^3} \frac{\mu}{c} \omega^2 \sin^2 \theta 4T^2 \frac{\sin^2 \omega HT}{2} |\hat{\rho}_0'(\hat{n}\omega/c)|^2 \quad (\text{A12})$$

$W$  is the energy radiated per unit solid angle per unit angular frequency,  $\omega$ . To proceed to the total energy, multiply by  $d\Omega$  (solid angle) and integrate. But  $n_z = \cos \theta$  so that  $d\Omega$  may be related to  $dH$ :

$$d\Omega = d(\cos \theta) d\Omega = -\frac{c}{v} dH d\Omega \quad (A13)$$

The function in equation (A12) does not contain  $\theta$ ; so that integration over  $\theta$  yields  $2\pi$ . Thus:

$$W(\omega, n) d\Omega = \frac{1}{2\pi^2} \frac{\mu}{v} \omega^2 T^2 / \sin^2 \theta_C |_{\theta_0'} \left( \frac{\sin^2 \omega H T}{(\omega H T)^2} dH \right) \quad (A14)$$

The  $\sin^2 \omega H T / (\omega H T)^2$  factor in the integral is peaked at  $H = 0$ , which, by equation (A9), is at  $n_z = \cos \theta = \frac{c}{v}$ , or the usual Cerenkov angle,  $\theta_C$ . This function is more strongly peaked about  $H = 0$  for large values of  $T$ , and in fact, for large  $T$  we may evaluate  $\sin^2 \theta$  and  $\theta_0'$  at the point corresponding to  $H = 0$ . Then the integral

$$\int_{-\infty}^{\infty} dx \sin^2(ax)/(ax)^2 = \pi/a$$

may be used to evaluate equation (A14), yielding

$$\iint W d\Omega = \frac{\mu}{4\pi} \frac{\omega}{v} 2T \sin^2 \theta_C |_{\theta_0'} \left( \frac{\hat{n}\omega/c}{\hat{n}\omega/c + 1} \right)^2 \quad (A15)$$

The emission was assumed to occur in a time interval from  $-T$  to  $T$ , accordingly involving  $2T$  in the rate calculation,

and multiplying by  $v$  converts to emission per unit path length. Thus we obtain, for the large  $T$  limit:

$$\frac{d^2 E}{dx d\omega} d\omega = \frac{\mu}{4\pi} \omega d\omega \sin^2 \theta_c |\rho'_0(\hat{n}\omega/c)|^2 \quad (A16)$$

where  $d^2 E/d\omega dx$  is the energy emitted per unit path length per unit angular frequency range  $\omega$ .

The corresponding expression for  $T$  not large is

$$\frac{d^2 E}{dx d\omega} d\omega = \frac{\mu}{4\pi} \omega d\omega \left(\frac{\omega T}{\pi}\right)^2 \int_{H'}^{H''} \sin^2 \theta |\rho'_0(\hat{n}\omega/c)|^2 \frac{\sin^2 \omega HT}{(\omega HT)^2} \quad (A17)$$

where  $H''$  and  $H'$  are the value of  $H$  corresponding to  $\theta = 0$  and  $\theta = \pi$  respectively.

Equations (A16) and (A17) then describe the energy radiated per unit path length and per unit angular frequency range. For the non periodic (single) pulse the radiation has a continuous frequency spectrum. For a point charge  $q$ ,  $\rho'_0(\vec{k})$  is identically  $q$  and the usual Cerenkov formula is obtained. Equation (A16) is quoted by Jelly, but only with the form factor corresponding to a uniform line charge of length  $L'$  [Ref. 3].

APPENDIX B  
DERIVATION OF EQUATION 7

Equation 7 is derived for the case in which  $\vec{J}(\vec{r}, t)$  is expanded in Fourier series. Let the Fourier coefficient for  $\vec{A}$  be given by:

$$\vec{A}(\vec{r}, \omega) = \frac{1}{\tau} \int_0^{\tau} dt \vec{A}(\vec{r}, t) e^{i\omega t} \quad (B1)$$

Assume that the Green's function solution for  $\vec{A}(\vec{r}, t)$  is given as:

$$\vec{A}(\vec{r}, t) = \iiint d^3 r' / dt \vec{J}(\vec{r}, t) D(\vec{r}-\vec{r}', t-t') \quad (B2)$$

where

$$D(\vec{r}, t) = \frac{1}{4\pi r} \delta(t - r/c) \quad (B3)$$

Let the current density be expanded in a Fourier series:

$$\vec{J}(\vec{r}', t') = \sum_{\omega'} e^{-i\omega' t'} \vec{J}(\vec{r}', \omega) \quad (B4)$$

Then insert (B2), (B3) and (B4) into (B1) to obtain

$$\tilde{A}(\vec{r}, \omega) = \frac{\mu}{\tau} \int_0^{\tau} dt e^{i\omega t} \iiint d^3 r' \int dt' \frac{1}{4\pi} \frac{1}{|\vec{r} - \vec{r}'|} \quad (B5)$$

$$\delta(t-t'-|\vec{r}-\vec{r}'|/c) \sum_{\omega'} e^{-i\omega't'} \tilde{J}(\vec{r}', \omega')$$

Do  $\int_0^{\infty} dt'$ , note that  $t'$  appears in the  $\delta$  function and in  $e^{-i\omega't'}$ . The result is  $t'$  is evaluated at  $t' = t - |\vec{r}-\vec{r}'|/c$ .

$$\tilde{A}(\vec{r}, \omega) = \frac{\mu}{\tau} \int_0^{\tau} dt e^{i\omega t} \iiint d^3 r' \frac{1}{4\pi} \frac{1}{|\vec{r} - \vec{r}'|} \quad (B6)$$

$$\sum_{\omega'} e^{-i\omega't} e^{i\omega|\vec{r}-\vec{r}'|/c} \tilde{J}(\vec{r}', \omega')$$

Do the integral on  $t$ , note that

$$\frac{1}{\tau} \int_0^{\tau} dt e^{i(\omega-\omega')t} = \delta_{\omega', \omega} \quad (B7)$$

Then do the sum on  $\omega'$

$$\tilde{A}(\vec{r}, \omega) = \frac{\mu}{4\pi} \iiint d^3 r' \frac{1}{|\vec{r} - \vec{r}'|} \tilde{J}(\vec{r}', \omega) e^{i\omega|\vec{r}-\vec{r}'|/c} \quad (B8)$$

This proves the desired result, (B8) is equation 7 as used in the main text.

A

**APPENDIX C**  
**CALCULATIONS**

In an earlier experiment at the Naval Postgraduate School LINAC, Leslie J. Brown [Ref. 4] showed that for small  $\phi_0'$

$$\frac{\phi_0^2}{2} = \frac{\Delta \epsilon}{\epsilon_0} \quad (C1)$$

where  $\epsilon$  is the electron energy.

Let linear accelerator be set for  $\frac{\Delta \epsilon}{\epsilon_0} = 10^{-2}$ , so that

$$\phi_0' = \pm \sqrt{2} \times 10^{-1} \text{ rad.} \quad (C2)$$

$$\frac{2\phi_0'}{2\pi} = 4.5 \times 10^{-2} \quad (C3)$$

This means that electrons are accepted 4.5% of each cycle. Our LINAC Klystrons operate at 2.856 GHz ( $\lambda = 10.5$  cm),

$$.045/2.856 \text{ GHz} = 16 \text{ p. sec.} \quad (C4)$$

Therefore, the LINAC produces bunches that are 16 picoseconds long. Incidentally, it does so in one microsecond burst at the rate of 60 bursts per second.

Figure 20 is a sketch of the beam current for simplicity it is assumed that the current is constant over its 16 psec. on time, rather than having some more complicated shape.

In theory, it is assumed that the charge distribution for a single pulse be given by Gaussian functions

$$\rho_0(r) = A \exp(-x^2/a^2 - y^2/a^2 - z^2/b^2)$$

$$\approx A \exp\left(-\frac{\omega^2}{2} \frac{b^2}{4}\right) \quad (C5)$$

so it can be assumed that

$$2b = .4725 \text{ cm}$$

$$b = .23625 \text{ cm} \quad (C6)$$

The condition for an electron bunch is shown in Figure 21 noting that  $I_{\text{meter}} \approx 2 \times 10^{-8}$  Amps.

$$I_1 = I_{\text{meter}} \cdot \frac{1}{10^6} = 3.3 \times 10^{-7} \text{ Amp.} \quad (C7)$$

During 1 psec. pulse current ( $I_2$ ) is

$$I_2 = I_1 \times \frac{1}{60 \times 10^{-6}} = 5.55 \times 10^{-3} \text{ Amps} \quad (C8)$$

Using the relationship between  $I_2$  and  $q$  (total charge per bunch),

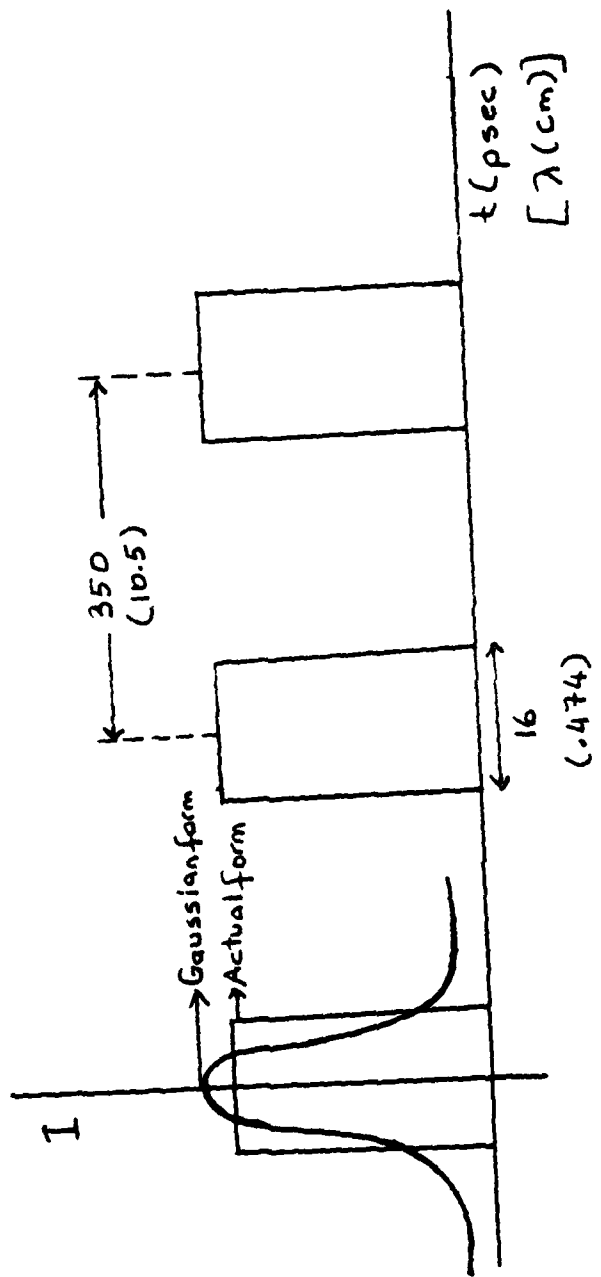


Figure 20. Beam Current as a Function of Time

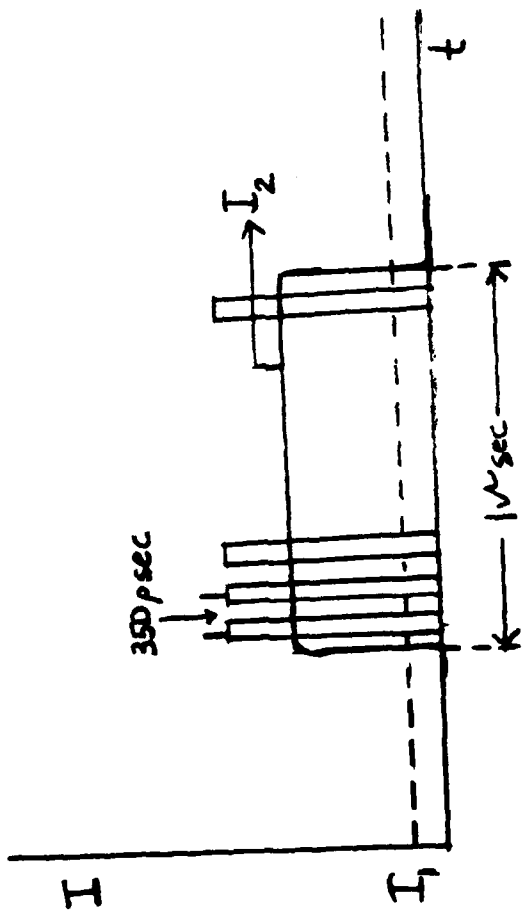


Figure 21. Relation Between Observed and Actual Beam Current

$$q = \frac{I_2}{2.856 \times 10^9} = 1.94 \times 10^{-12} \text{ Coulomb} \quad (\text{C9})$$

was found.

In the present case, experiments are conducted in air for electron energies  $\approx 100$  MeV. Corresponding values are for these experimental conditions:

$$n = \text{refractive index of air} = 1.00036$$

$$\mu = \text{permeability constant of air} = 1.256 \times 10^{-6} \text{ Henry/m}$$

$$c_0 = \text{speed of radiation in vacuum} = 2.998 \times 10^8 \text{ m/sec}$$

$$B = .999987$$

$$c = \text{speed of radiation in air} = \frac{c_0}{n} = 2.997 \times 10^8 \text{ m/sec}$$

$$v = \text{speed of electrons} = 3 c_0 = 2.9978 \times 10^8 \text{ m/sec}$$

The relationship between  $d\Omega$  and area of an antenna is

$$d\Omega_{\text{ant}} = \frac{\text{area}}{(L_1 + L_2/2)^2} \quad (\text{C10})$$

The X Band antenna has dimensions  $4.6 \text{ cm} \times 3.15 \text{ cm}$  and K Band antenna has dimensions  $7.2 \text{ cm} \times 5.75 \text{ cm}$ . Results are shown in Table 10.

The cut-off frequency of the X Band wave guide is 6.56 GHz, and cut off frequency of the K Band wave guide is 14.08 GHz. So all the calculations for the X Band begins from the third harmonic, and for the K Band, from the fifth harmonic.

TABLE 10

	Area (cm <sup>2</sup> )	L <sub>1</sub> (cm)	L <sub>2</sub> (cm)	dΩ
X Band	14.49	88.9	99.06	$7 \times 10^{-4}$
X Band	14.49	66.04	10.16	$8 \times 10^{-4}$
X Band	14.49	109.22	114.3	$5 \times 10^{-4}$
K Band	41.4	88.9	99.06	$20 \times 10^{-4}$
K Band	41.4	66.04	101.6	$23 \times 10^{-4}$
K Band	41.4	109.22	114.3	$14.5 \times 10^{-4}$

APPENDIX D  
FORTRAN PROGRAM LISTINGS

To solve the equations (25) and (26), three Fortran computer programs were used.

1. FORTRAN 1 solves  $I^2$  as a function of  $\theta$  for one particular frequency.

2. FORTRAN 2 solves  $dP/d\Omega$  as a function of  $\theta$  for one particular frequency.

3. FORTRAN 3 solves  $\int_{N_1}^{N_2} dP/d\Omega$  as a function of  $\theta$ .

In the first and second programs, responses can be found for other harmonics by making a change from  $N = 3$  to  $N =$  Desired harmonic number. In the third program, making a change from  $K = 3,10$  to  $K =$  Desired harmonic numbers.

The corresponding program and theoretical symbols are shown in Table 11.

TABLE 11

<u>Program Symbol</u>	<u>Theoretical Symbol</u>
$z_1$	$z'$
PI	$\pi$
$w_0$	$\omega_0$
v	$v$
c	$c$
Q	$\frac{\mu \omega_0^2 v^2 c^2}{\tau z^2 c^2}$
2.1024900449	$\frac{1}{2} \left( \frac{\omega_0 b}{c} \right)^2$
-0.01000480877	

1) FORTRAN program 1

```
//AHMETI3 JOB (2075,1000),'ATILLAX',CLASS=A
// EXEC FRTXCLGP,REGION.GD=300K
//FORT.SYSIN DD *
      REAL*8 TITLE(12)
      REAL*8 LABEL/'   /
      REAL X(1100),Y(1100),Q1(1100)
      REAL W0,V,C,Z1,PI,N,Q,
      READ(5,105)(TITLE(J),J=1,6)
      READ(5,105)(TITLE(J),J=7,12)
105  FORMAT(6A8)
      Z1=.4445
      PI=3.14159263
      N=3.
      W0=17.94477724*(10**9)
      V=2.997886027*(10**8)
      C=2.997025892*(10**8)
      X(1)=0.
      DO 10 I=1,991
          Q1(I)=X(I)-22.
          Q=PI/180.*Q1(I)
          A=N*Z1*(W0/V-W0*COS(Q)/C)
          B1=SIN(A)*2.
          G=(N*(W0/V-W0*COS(Q)/C))
          F=B1/G
          Y(I)=F**2
          X(I+1)=X(I)+0.043
10    CONTINUE
      CALL DRAW(990,Q1,Y,0,0,LABEL,TITLE,
      10.,0.,0.,0.,0.,4,4,1,LAST)
      WRITE(6,25)
      WRITE(6,100)(Q1(I),Y(I),I=1,990,10)
100  FORMAT(12X,E16.7,10X,E16.7)
25   FORMAT('1',15X,'ANGLE',21X,'ISQUARE')
      STOP
      END
//GO.SYSIN DD *
      ANGLE VERSUS
      I SQUARE(N=3)
```

2) FORTRAN program 2

```

//SAGLAM3 JOB (2075,1000), "AHMETX",CLASS=A
//EXEC FRTXCLGP,REGION.GC=300K
//FORT.SYSIN DD *
      REAL*8 TITLE(12)
      REAL*8 LABEL/*   */
      REAL X(1100),Y(1100),Q1(1500)
      REAL W0,V,C,Z1,PI,N,Q
      READ(5,105)(TITLE(J),J=1,6)
      READ(5,105)(TITLE(J),J=7,12)
105  FORMAT(6A8)
      Z1=.4445
      PI=3.14159263
      N=3
      W0=179.4477724*(10**9)
      V=2.997886027*(10**8)
      EXP=2.718281828
      C=2.997025892*(10**8)
      X(1)=0.
      DO 10 I=1,991
         Q1(I)=X(I)-22.
         Q=PI/180.*Q1(I)
         A=N*Z1*(W0/V-W0*COS(Q)/C)
         B1=SIN(A)
         B=B1**2
         G=(N*Z1*(W0/V-W0*COS(Q)/C))**2
         D=2.1024966449*((N*SIN(Q)*Z1)**2)
         E1=-0.01000480877*((N*COS(Q))**2)
         E=EXP**E1
         F=B/G
         Y(I)=E*F*D
         X(I+1)=X(I)+0.043
10    CONTINUE
      CALL DRAW(990,Q1,Y,0,0,LABEL,TITLE,
      10.,0.,0.,0.,0.,4,4,1,LAST)
      WRITE(6,25)
      WRITE(6,100)(Q1(I),Y(I),I=1,990,10)
100  FORMAT(10X,E16.7,5X,E16.7)
25   FORMAT('1',15X,'ANGLE',16X,'DP/DCMega')
      STOP
      END
//GO.SYSIN DD *
      ANGLE VERSUS
      DP/DCMega (N=3)

```

3) FORTRAN program 3

```

//SELMA JDB ( 2075,1000), 'SELMAX', CLASS=A
// EXEC FRTEXCLGP, REGION.GD=300K
//FORTRAN.SYSIN DD *
      REAL*8 TITLE(12)
      REAL*8 LABEL//      /
      REAL X(1100),Y(1100),Q1(1500),PZ(25)
      REAL W0,V,C,Z1,PI,N,Q,T(1100)
      READ(5,105)(TITLE(J),J=1,6)
      READ(5,105)(TITLE(J),J=7,12)
105 FORMAT(6A8)
      Z1=.4445
      DO 12 L=1,995
      T(L)=0.
12 CONTINUE
      PI=3.14159263
      W0=179.4477724
      V=2.997886027
      EXP=2.718281828
      C=2.997025892
      DO 10 K=3,10
      N=FLCAT(K)
      X(1)=0.
      DO 20 I=1,995
      Q1(I)=X(I)
      Q=PI/180.*Q1(I)
      A=N*Z1*(W0/V-W0*COS(Q)/C)
      B1=SIN(A)
      B=B1**2
      G=(N*Z1*(W0/V-W0*COS(Q)/C))**2
      D=2.1024966449*((N*SIN(Q)*Z1)**2)
      E1=-0.01000480877*((N*COS(Q))**2)
      E=EXP**E1
      F=B/G
      Y(I)=E*F*D
      X(I+1)=X(I)+0.05
      T(I)=T(I)+Y(I)
20 CONTINUE
10 CONTINUE
      CALL DRAW(995,Q1,T,0,0,LABEL,TITLE,
      10.,0.,0.,0.,0.,0.,4,4,1,LAST)
      WRITE(6,25)
      WRITE(6,100)(Q1(I),T(I),I=1,990,10)
100 FORMAT(10X,E16.7,5X,E16.7)
25 FORMAT('1',15X,'ANGLE',18X,'DPT/DOMEGA')
      STOP
      END
//GO.SYSIN DD *
ANGLE VERSUS
TOTAL DP/DOMEGA (N=3,10)

```

LIST OF REFERENCES

1. Engineering Staff of the Microwave Division of Hewlett-Packard, Microwave Theory and Measurements, Prentice-Hall, 1962.
2. Love, A.W., Electromagnetic Horn Antennas, p. 138-140, IEEE Press, 1976.
3. Jelly, J.V., Cerenkov Radiation and Its Applications, Pergamon Press, London, 1958.
4. Brown, L.J., Stimulated Cerenkov Produced by 100 MeV Electrons, Master's Thesis, Naval Postgraduate School, Monterey, 1981.

INITIAL DISTRIBUTION LIST

	No. Copies
1. Defense Technical Information Center Cameron Station Alexandria, Virginia 22314	2
2. Library, Code 0142 Naval Postgraduate School Monterey, California 93940	2
3. Physics Library, Code 61 Department of Physics and Chemistry Naval Postgraduate School Monterey, California 93940	2
4. Professor F.R. Buskirk, Code 61Bs Department of Physics and Chemistry Naval Postgraduate School Monterey, California 93940	10
5. Professor J.R. Neighbours, Code 61Nb Department of Physics and Chemistry Naval Postgraduate School Monterey, California 93940	2
6. LTJG Ahmet Saglam Havvzlubahce subay ev. Bahar apt. No: 1/3 Florya-Istanbul TURKEY	2
7. Deniz Kuvvetleri Komutanligi Egitim Dairesi Ankara, TURKEY	5